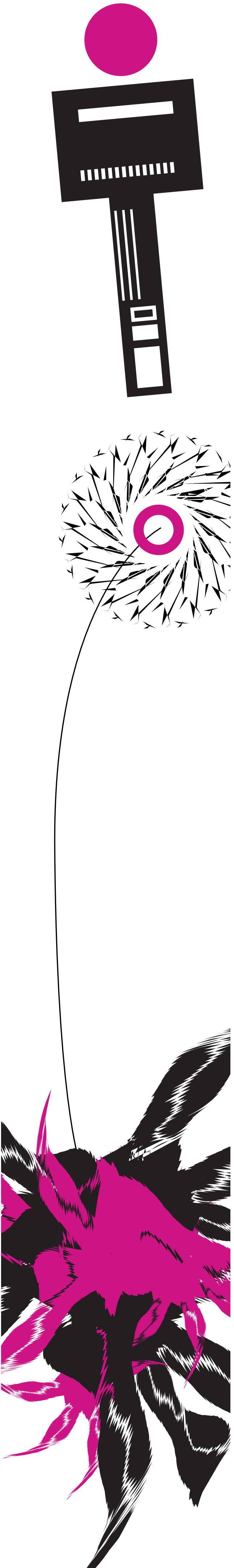

RAM ROBOTICS AND MECHATRONICS

RESEARCH INTO 3D PRINTED BATTERIES THROUGH ELECTRODEPOSITION

L. (Luka) Šćulac

BSC ASSIGNMENT

Committee:
prof. dr. ir. G.J.M. Krijnen
A.P. Dijkshoorn, MSc
dr. ir. W. Olthuis

November, 2019

050RaM2019
Robotics and Mechatronics
EEMathCS
University of Twente
P.O. Box 217
7500 AE Enschede
The Netherlands

UNIVERSITY OF TWENTE. | TECHMED CENTRE
UNIVERSITY OF TWENTE. | DIGITAL SOCIETY INSTITUTE

Abstract

In this study, the fabrication of a 3D printed battery through electrodeposition is attempted. The electroplated 3D printed battery consists of two dissimilar electroplated electrodes immersed into an electrolyte. Suitable materials and electrolyte had to be found that would allow the battery to be 3D printed without any assembly.

While research papers have already proven that electrically conductive 3D printed materials can be electroplated, there is a lack of research in utilizing the electroplated 3D printed materials as electrodes in a battery as well as a lack of research into the performance of such a battery.

The process of electrodeposition is used to deposit copper and zinc metal ions onto the two electrically conductive electrodes. A Galvanostat with a three electrode setup was used to keep the current stable and measure the current and voltage over time.

Once the 3D printed battery was fabricated, electrochemical impedance measurements were taken with an LCR meter and the discharge voltage and current measurements were taken with a multimeter. The 3D printed battery was attempted to be modelled by an equivalent circuit and its discharge graph compared with other currently researched batteries.

In the end, the 3D printed battery was fabricated and achieved a rated capacity of 6.6 mAh. However, given the voltage potential of approximately 0.9 V, the 3D printed battery has high internal resistance. Furthermore, issues with the electrolysis of the solution hindered the performance of the 3D printed battery.

Contents

1 Introduction

1.1 Context

More cost-effective and power efficient technologies for energy storage are at the forefront of research and development in today's world [Pickerel et al., 2019, Pocket-lint, 2019, 1bu, 2019, Dudley, 2018]. With an ever-increasing human population, the manufacturing capacity of energy storage devices is heavily lagging behind the demand as a recent study predicts that the number of energy storage installments will have to increase by a 122-fold to meet demand by 2040 [Editors, 2019]. Therefore, entities such as private companies and public universities have been researching and developing alternative methods for the fabrication of energy storage devices [Waugh, 2013, Wikipedia contributors, 2019g].

One such fabrication process exists in the form of 3D printing, which embodies the entire manufacturing process into one system that allows for complex free-form geometries and controllable 3D structural prototyping [Tian et al., 2017]. 3D printed energy storage devices primarily function on the concept of captured electrical energy, which is achieved through either the electric domain with the use of a dielectric or the electrochemical domain with the use of an electrolyte or a combination of the two in the case of the supercapacitor [Zhang et al., 2017a]. In the past, the materials available for 3D printing were limited to rigid plastics such as PLA and ABS. With recent advancements, composite materials have been developed that possess the property of electrical conductivity through the addition of additives such as copper and carbon-black particles [Schouten, 2017, Kim et al., 2016]. In turn, these composite materials can be printed into stand-alone structures in such a way that they become 3D printed energy storage devices such as capacitors and supercapacitors.

With the use of 3D printing and electrically conductive filaments, electrolytic capacitors have been fabricated with more complex geometries, i.e. maze-like and interdigitated patterns, in the efforts to maximize the effective surface area of the two conductive sides [Esfandiari et al., 1983]. On the other hand, supercapacitors, first introduced in the 1950s, have the advantage of storing 10 to 100 times more energy per unit volume than electrolytic capacitors, having faster charging and discharging cycles than batteries, and tolerating more charge and discharge cycles than rechargeable batteries; they owe these advantages to the inclusion of an electrolyte that forms an ionic conductive connection between the two electrodes, which differs from the constant dielectric layer found in electrolytic capacitors [Wikipedia contributors, 2019j]. Generally, there are two different types of supercapacitors that each rely on a different kind of capacitance: electrostatic double-layer capacitance and electrochemical pseudo-capacitance; in the first type, capacitance is created through the separation of charge in a Helmholtz double layer at the interface between the conductive electrode and electrolyte; in the second type, capacitance is created through the Faradaic electron charge transfer, which is achieved through either redox reactions, intercalation, or electrosorption [Wikipedia contributors, 2019j]. As with electrolytic capacitors, the research in terms of 3D printed supercapacitors has been focused on finding geometries for the electrodes that maximize the effective surface area as well as increasing the capacitance through doping and activation of carbon black particles within the composite filaments [Tiliakos et al., 2018, Beidaghi and Gogotsi, 2014, Zhang et al., 2014, Zhao et al., 2014, Yu et al., 2018, Sun et al., 2015].

However, supercapacitors still lack the capacity of batteries as, in most cases, supercapacitors contain only one-tenth of the capacity [Wikipedia contributors, 2019j]. Current commercially available electrically conductive filament is not sufficient to 3D print a fully-functioning battery without additional additives; electric batteries require redox reactions that result from the insertion of two dissimilar metal electrodes into an electrolyte [Wikipedia contributors, 2019c].

At the current moment, there is quite extensive research on the topic of 3D printed batteries with two distinctive paths of focus; some papers develop techniques for 3D printing the entire battery while others focus on tackling the issue of 3D printing individuals components of the battery such as the electrodes and electrolytes [Shen et al., 2017, Garay and Bashirullah, 2015, Ho et al., 2009, Down et al., 2019, Lawes et al., 2015]. To 3D print the entirety of the battery without post-processing, some studies prepared the filament prior to printing, i.e. by dissolving standard PLA filament into a solution containing either lithium iron phosphate or lithium titanium oxide to create two dissimilar metal electrodes; then, through this process, these papers utilize standard printers to print embedded batteries within structural components [Reyes et al., 2018, Wang et al., 2017]. Furthermore, other publications on 3D printed batteries focus on the individual methods used to 3D print electrodes and electrolytes; in terms of electrodes, the focus has been on testing the printability of different materials such as lithium and graphene and evaluating their ionic conductivity [Walsh et al., 2018, Rocha et al., 2017, Liu et al., 2017, Yi et al., 2018]; in regards to electrolytes, the focus has been on developing 3D printable solid-state ceramic composite electrolytes that maintain high ionic conductivity and mitigate brittleness [Blake et al., 2017, Mcowen et al., 2018, Zekoll et al., 2018].

However, most of the methods shown in these papers require extensive equipment and preparation to the filament and 3D printer itself. As mentioned earlier, it is possible to 3D print carbon and other electrically conductive composite materials, but metals are required for electrochemistry. One alternative solution exists in the form of electrodeposition, which is a process that deposits metal ions through the application of an electric current [Kanani, 2006]. Unlike electroless plating that relies solely on chemical reactions and covers the entirety of the surface area, electrodeposition can be done selectively, making it possible to only cover the areas desired. In conjunction with 3D printing, electrodeposition would enable the deposition of different metals onto separate electrically conductive areas that are already embedded within the same 3D printed part, thereby mitigating any assembly on part of the electrodes [Angel et al., 2018].

Previously published papers have already successfully proven the concept of electroplating metal ions on an electrically conductive 3D printed part [Kadari, 2017, Zhang et al., 2017b, Angel et al., 2018, Kim et al., 2019, Dhole et al., 2018, Sonavane et al., 2010, Felloni et al., 1987]. However, there is inadequate research on the topic of utilizing 3D printed electrically conductive parts that have been electroplated as electrodes for a 3D printed battery; also, there is insufficient research on the performance of such a battery.

The 3D printed battery would require two different metals to be electroplated onto the 3D printed electrodes. As mentioned earlier, it has already been proven that lithium can be electroplated onto electrically conductive 3D printed materials [Zhang et al., 2017b]. However, these methods to electroplate lithium and their composites require extensive preparation of the electroplating solution and modification of the equipment setup. Alternatively, among other options of metals that are commonly electroplated such as nickel, iron, copper, zinc, silver, etc., one possibility lies in the combination of nickel and zinc, whose chemistry is utilized to create rechargeable batteries. However, the option to fabricate a rechargeable 3D printed battery is outside the true scope of the thesis as the focus should be on developing the most basic type of battery to answer the research goals of this thesis in their most basic form. Furthermore, time constraint and availability of resources and equipment are other factors to consider as well.

The metal pair combination of copper and zinc was ultimately chosen due to the simplicity of the composition of the final electroplated electrodes and the relatively inexpensive and straightforward electrodeposition process.

1.2 Research Goals

Thus, in this thesis, a fully-functioning 3D printed battery will be envisioned through the use of electrodeposition. The 3D printed battery will consist of the 3D printed part with its two electroplated electrodes immersed into an electrolyte. With this clear objective, the main research question becomes:

- **How does the performance of a 3D printed battery fabricated with the use of electrodeposition compare with currently researched batteries?**

Furthermore, the thesis will focus on the 3D printing of electrically conductive and non-conductive materials as well as the characterization of the behavior between the electroplated electrodes and electrolyte. Therefore, the following sub-questions arise:

- What is the optimal configuration of the 3D printed electrodes that will permit the best coverage of metal ions during the electrodeposition process?
- What is the ideal electrolyte that will allow for the largest battery capacity?
- How can the electrical characteristics of the 3D printed battery be modelled?

To answer these questions, the thesis will follow the structure outlined in the following section.

1.3 Report Structure

As witnessed earlier, Chapter 1 was the introduction to the thesis and provided the literature overview along with the main goals of the report.

Chapter 2 contains the general theory needed for this thesis and will cover the basic understanding of the chemistry of an electric battery and the process of electrodeposition.

Chapter 3 contains the reasoning behind the design choices of the 3D printed battery.

Chapter 4 discusses the characterization methods that will be used to characterize the battery.

Chapter 5 contains the methodology and provides insight into the methods used to fabricate the 3D printed battery.

Chapter 6 constitutes the results and discussion section of the thesis and will therefore cover the results of the electrodeposition of the electrodes as well as the characterization of the finished 3D printed battery.

Chapter 7 concludes the thesis by answering the research goals stated in Chapter 1 and provides a summary on future improvements.

2 Theory

In this chapter, the theory behind the the basis of the chemical reactions that produce a measurable electric current at the output of a battery will be explained as well as the process of electrodeposition. In addition, the aspects of 3D printing that enable the fabrication of the 3D printed battery will be mentioned.

2.1 Redox Reactions

As briefly mentioned in the introduction, an electric battery operates on the principle of redox reactions, which release electrical energy from the difference in the bond energies of the metals present in the battery [Wikipedia contributors, 2019i]. More specifically, there are two types of redox reactions: oxidation and reduction. Oxidation is the result of a decrease in the oxidation state of the atoms, or a net loss of electrons [Wikipedia contributors, 2019i]. Reduction, on the other hand, is the result of an increase in the oxidation state of the atoms, or a net gain of electrons [Wikipedia contributors, 2019i]. Thus, an exchange of electrons occurs through the process of oxidation and reduction till the high-energy reactants in the battery become lower-energy products.

For oxidation and reduction to occur, a closed loop between the two separate metal electrodes has to exist to facilitate the movement of electrons and metal ions. Within the battery, the electrolyte envelopes the two metal electrodes and serves as a medium for the oxidized metal ions to enter and reduced metal ions to leave. Externally, the two metal electrodes are connected with a wire, which allows the transfer of electrons from the electrode where oxidation happens to the electrode where reduction occurs.

An example of the basic principle of the redox reactions can be seen in Figure 2.1.

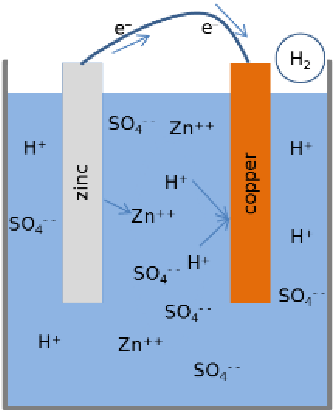

Figure 2.1: Cross-section of a copper-zinc battery with sulfuric acid electrolyte [Wikipedia contributors, 2019h]

As can be seen in Figure 2.1, the example is a copper-zinc battery with sulfuric acid as the electrolyte. With reduction happening at the cathode and oxidation occurring at the anode, the copper-zinc battery constitutes what is called a Galvanic cell. On the left side of the battery in Figure 2.1, the zinc metal from the zinc anode is oxidized according to the following half-reaction:

$\mathrm{Zn(s)} \longrightarrow \mathrm{Zn^{2+}(aq)} + 2\,\mathrm{e^-}$

The electrons freed from the oxidation of the zinc metal pass through the wire to the copper electrode while the freed zinc ions enter the electrolyte. At the same time, on the right side of the battery in Figure 2.1, the hydrogen ions within the electrolyte are reduced according to the following half-reaction:

$$2\,\mathrm{H}^+ + 2\,\mathrm{e}^- \longrightarrow \mathrm{H}_2$$

The electrons that have passed through the wire from the zinc electrode now reside on the surface of the copper electrode and attract the hydrogen ions from the solution, ultimately bonding and bubbling away as hydrogen gas [Wikipedia contributors, 2019h]. Thus, the total reaction can be summarized by [Wikipedia contributors, 2019h]:

$$\mathrm{Zn(s)} + 2\,\mathrm{H}^+ \xrightarrow{2\,\mathrm{e}^-} \mathrm{Zn}^{2+}\mathrm{(aq)} + \mathrm{H}_2$$

Generally, with the knowledge of the half-reactions, it is possible to calculate the open circuit voltage by adding the absolute value of the standard electrode reduction potentials. However, in the case of strong acids, the Nernst equation cannot predict the standard electrode potential [Wikipedia contributors, 2019h].

Apart from the single electrolyte configuration, the copper-zinc battery also comes in the form of two half-cells, also known as the Daniell cell. The basic principle of the Daniell cell can be seen in Figure 2.2. In the zinc half-cell, a zinc anode is submerged in a solution of zinc sulfate. In the copper half-cell, a copper cathode is submerged in a solution of copper sulfate. Both half-cells are connected by means of a wire and salt bridge. The wire permits the passage of electrons while the salt bridge allows for only the passage of ions. The salt bridge can be a glass tube filled with an inert electrolyte or a porous membrane, i.e. filter paper [Wikipedia contributors, 2019b].

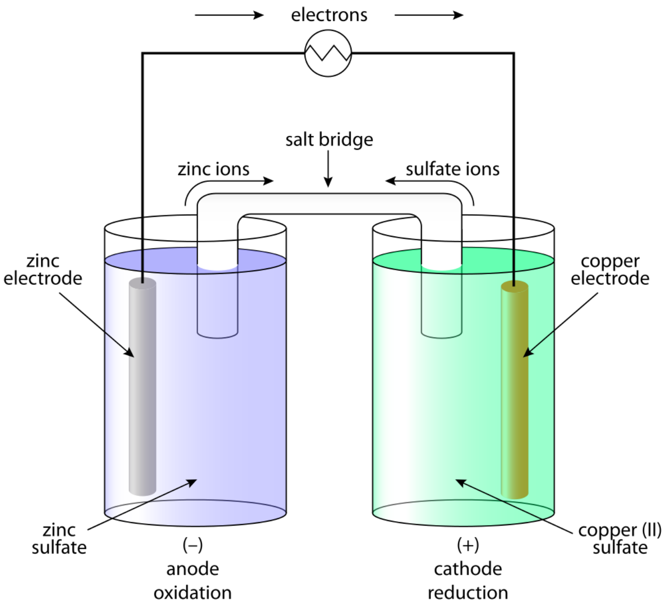

Figure 2.2: A diagram of a standard Daniell cell with its two half-cells connected by a salt bridge [Wikipedia contributors, 2019b]

The zinc metal still participates in the process of oxidation, but, now, the copper metal undergoes reduction instead of the hydrogen molecules within the electrolyte.

In the following section, the fundamentals of electrodeposition will be given.

2.2 Electrodeposition

To obtain the electrodes that will be used in the final 3D printed battery, the process of electrodeposition was used. As briefly articulated in the introduction, electrodeposition involves the application of an electric current on two submerged electrodes to ultimately coat one of the two electrodes with dissolved metal ions from the solution through reduction [Wikipedia contributors, 2019e].

Despite the electrodeposition process being slightly different for copper and zinc, the basic concept is the same. As can be seen in Figure 2.3, the anode and cathode are immersed into a solution that contains dissolved ions of the metal to be electroplated. The chemical reactions that happen during electrodeposition are analogous to a Galvanic cell acting in reverse; instead of oxidation happening at the anode, reduction occurs during electrodeposition and vice-versa for the cathode [Wikipedia contributors, 2019e]. Therefore, the rate at which the metal ions from the cathode are dissolved into the electrolyte is equal to the rate at which the anode is plated. As a result, it is important to make sure that both the cathode and electrolyte contain the metal that will electroplated as the metal from the cathode replenishes the supply of metal ions in the electrolyte during the electrodeposition process [Kanani, 2006].

Since both copper and zinc have to be electroplated, a copper cathode in a copper sulfate solution with dissolved copper ions will be used for the copper electrodeposition and a zinc cathode in a zinc sulfate solution with dissolved zinc ions will be used for the zinc counterpart.

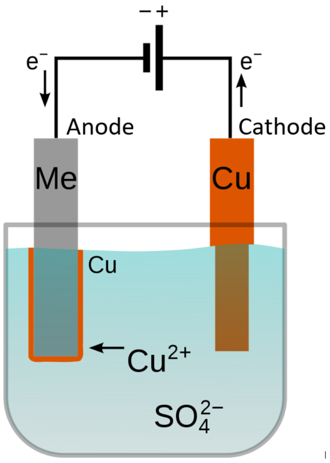

Figure 2.3: A diagram showcasing the electrodeposition of copper with a solution of copper sulfate [Wikipedia contributors, 2019e]

Likewise, for the electrodeposition processes to be successful, the copper and zinc ions in the electroplating solution require a certain current to supply enough electrons on the surface of the anode to bond with. The required current follows a upward linear trend with the surface area of the anode. The current density for copper electrodeposition is $3\,\mathrm{mA/cm^2}$. Meanwhile, the current density for zinc electrodeposition is $20\,\mathrm{mA/cm^2}$.

In the next section, it will be explained how the current can be kept constant, despite the drop in the electrical resistance of the electroplated electrode.

2.2.1 Three Electrode Setup

To drive the whole electrodeposition process, it is important to have a stable, steady flow of electrons through the anode, electrolyte, and cathode. Normally, a voltage source would be attached to the ends of the anode and cathode; however, due to the high resistance of the electrically conductive 3D printed material, very little current would be permitted to flow. The electrical resistivity and conductivity of the 3D printed material and its respective impact on the behavior of the 3D printed battery will be examined in further detail in Chapter 3.

Rather, a current source should be used to ensure that the desired current is being supplied to the whole system. To maintain the current density specified previously, a Galvanostat will be used since it is a control and measuring tool capable of keeping the current constant through an electrolytic cell, regardless of the changes in the load itself thanks to to its relatively infinite internal resistance [Wikipedia contributors, 2018]. Thus, as the electrically conductive 3D printed electrode is being electroplated and its electrical resistance decreases, the voltage drop over the anode will decrease. As a result, the Galvanostat responds to the change in the electric resistance by varying its output potential.

To gain an unbiased measurement of the voltage potential within the electrolytic cell, the Galvanostat relies on a three electrode setup, which consists of a working, reference, and counter electrode as can be seen in Figure 2.4. The term "working electrode" is another label for the anode, or the electrically conductive 3D printed electrode on the 3D printed part. The term "counter electrode" refers to the cathode, or the electrode that is composed of the metal that is to be electroplated onto the working electrode. The third electrode, or reference electrode, does not directly participate in the electrodeposition process and is placed some distance from the other two electrodes; it is usually composed of non-reactive materials such as silver-chloride to provide an unbiased measurement of the voltage potential.

The correct wiring and orientation of the three electrodes with the Galvanostat will be mentioned later on in Chapter 5. If the electrodes are connected incorrectly, the current from the power supply will flow through the wrong components, resulting in no deposition at all and in most cases, failure of equipment.

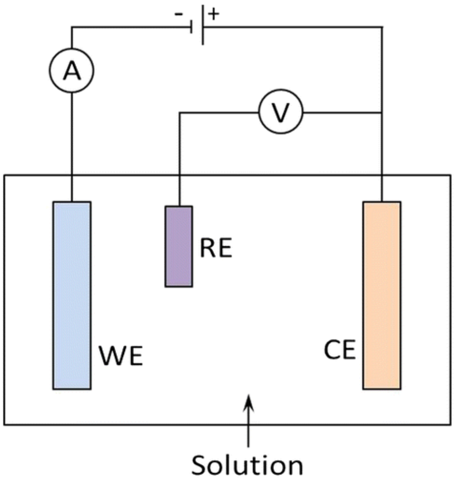

Figure 2.4: A diagram of a three electrode setup with the label "WE" for working electrode, the label "RE" for the reference electrode, and the label "CE" for counter electrode [Vangari et al., 2013]

In regards to the Galvanostat, another advantage of keeping the current constant is the ability to calculate the amount of metal that will be electroplated onto the working electrode with Faraday's Law of Electrolysis, which will be explained in the following section.

2.2.2 Electrodeposition Rate Calculations

With the knowledge of the current applied and its duration, it is possible to calculate the expected quantity of metal ions that will be electroplated onto the working electrode using Faraday's Law of Electrolysis. Faraday's Law of Electrolysis states that the amount of material reduced or oxidized at the working electrode is directly proportional to the total conducted charge and can be represented through the following equation [Wikipedia contributors, 2019f]:

$$m = \frac{M \cdot Q}{z \cdot F} \tag{2.1}$$

In the above equation, m is the mass in grams of the metal that is electrodeposited on the working electrode; M is the molecular mass of the metal being electroplated in grams per mol; z is the number of valence electrons of the metal being electroplated; F is Faraday's constant with the value of $96\,485.332\,89\,\mathrm{C\,mol^{-1}}$; Q is the total electric charge that has passed through the entire system in coulombs and can be calculated using the following integral over time [Wikipedia contributors, 2019f]:

$$Q = \int_0^T I dt \tag{2.2}$$

Assuming a constant current, preliminary calculations for the copper and zinc electrodeposition can be made. Also, using the three electrode setup during the actual electrodeposition process, the integral of the current over time can be taken. The exact current values used for the electrodeposition process will be mentioned in Chapter 5. Then, the measured results will be compared with the expected values in Chapter 6.

2.2.3 Selective Electrodeposition

As expressed in Chapter 1, electrodeposition offers a unique advantage over other techniques such as electroless plating that would otherwise make the battery unattainable. Selective electroplating allows for the electrodeposition of different metals onto the same 3D printed part, given that the areas of electrically conductive material are separated by areas of electrically non-conductive material [Angel et al., 2018]. The selection of area is made through the connection of the electrode with the current-carrying wire.

An important remark for electrodeposition is that the current carrying wire does not make contact with the electroplating solution. Otherwise, the deposition of metal ions will happen on the wire itself. Rather, the current-carrying wire should be connected to the electrode through an external part of the electrode that is not in contact with the electroplating solution. Furthermore, selective electroplating will not work if contact is made between the two electrodes either through the contamination of the 3D printed part or the unintentional presence of the electroplating solution.

2.2.4 Electrolysis of electroplating Solution

During the review of the specific current densities for the copper and zinc electrodepositions, one issue that should be considered is the electrolysis of the electroplating solution. At the voltage potential of 2.01 V, the sulfate ions within the electroplating solution undergoes electrolysis, resulting in bubbles of oxygen molecules that severely affect the electrodeposition process by significantly increasing the electrical resistance.

2.3 3D Printing

3D printing was specifically chosen for its ability to produce multi-material objects with complex geometries and no post-processing. FDM printing has the unique ability of switching between different materials during the fabrication process of the desired object. Therefore, the user has direct control over the dimensions and weight of the structure of the object as well as the resolution of the quality of the final product. Furthermore, 3D printing is practical as it requires only one piece of equipment and a computer with the necessary program to convert the desired model into code for the 3D printer. Changes to the model can be made immediately and the object being 3D printed can be immediately stopped if a defection is noticed during the 3D printing process. Otherwise, with some other methods of manufacturing, flaws in the object will only be noticed after fabrication.

Due to the fact that the material is melted onto the build plate of the 3D printer, the original characteristics of the material are inadvertently altered. In regards to the electrically conductive composite materials, one particular quality that is altered is the electrical resistivity. During extrusion, the electrically conductive particles within the filament are rearranged, resulting in the material developing high, anisotropical resistivity [Schouten, 2017, Dijkshoorn et al., 2019]. Thus, the 3D printing orientation of the object will have an effect on the behavior of the electrical resistivity of the object. The effects will be discussed in Chapter 3.

In the following chapter, the design choices that ultimately lead to the final design of the 3D printed battery will be explained.

3 Design Choices

In this chapter, the design choices that lead to the final design and implementation of the 3D printed battery will be analyzed.

3.1 Basic Concept

Within the general scope of the design, the 3D printed battery could follow one of two choices. The first choice is outlined by the diagram in Figure 2.1, where two dissimilar metal electrodes are immersed into a single electrolyte. The second choice follows the example of the Daniell cell in Figure 2.2, where two half-cells that each contain a dissimilar metal electrode are connected by a porous membrane or salt bridge.

The proposed implementation of the two half-cells and salt bridge creates new challenges. To still comply with the concept of no assembly for the 3D printed electrodes, the 3D printed sample would have to be large enough to encompass two beakers full of electrolytes and incorporate the porous membrane within its structure. Currently, further research has to be done to investigate whether a porous 3D printable material exists that could act as the salt bridge. In the case that a porous material can be found, it would require the 3D printing of three different materials over just the two for the first choice.

By opting for the configuration with one electrolyte over the one with two, the focus can be put on developing a simple battery that functions. Likewise, the use of a single electrolyte enables more flexibility and freedom with the design of the electrodes. The electrodes can be spaced closer together to increase the passage of ions and the unit as a whole can be 3D printed in such a way that it fits comfortably within a standard-sized beaker to ease the electrodeposition process.

Therefore, the final concept for the 3D printed battery can be summarized as a single glass beaker that contains a 3D printed sample with two electrically conductive electrodes that are submerged in an electrolyte.

3.2 Choice of Material

For the fabrication of the electrodes, several electrically conductive filaments were available, varying in the degree of flexibility and electrical conductivity. The choices for the electrically conductive filaments can be seen in Table 3.1. The resistivities provided in the table are the values given by the manufacturers for the filament itself; the values of the 3D printed material vary according to the 3D printing settings and geometry of the 3D printed object [Schouten, 2017, Dijkshoorn et al., 2019].

Table 3.1: Table of the inventory of 3D printer filament [Schouten, 2017]

	PI-ETPU 95-250	BlackMagic Conductive TPU	ElectriFi	Proto-Pasta	PI-ETPU 85-700+
Electrical Resistivity ($\Omega\,\mathrm{cm}^{-1}$)	300	1.25	0.01	15	80
Material Composition	TPU with carbon particles	TPU with carbon particles	PLA with copper particles	PLA filled with carbon-black particles	TPU with carbon particles
Additional Remarks	250 percent strain	Degrade after several months of shelf-life	Fragileness leads to inconsistent resistivities		700% strain

As can be seen in Table 3.1, there are five options for the choice of electrically conductive material. Essentially, the materials are grouped into two categories: flexible and rigid. Among each group, there are contenders for the material with the lowest electrical resistivity. Among the rigid materials, ElectriFi is the clear winner while the BlackMagic Conductive TPU secures the spot among the flexible materials. However, both filaments are excluded as viable options. The BlackMagic Conductive TPU has been removed from the market due to problems with its shelf-life and ElectriFi easily loses electrical conductivity in areas under strain due to its brittleness [Schouten, 2017].

The electrically conductive filament that was chosen was Proto-Pasta due to its low electrical resistivity when compared to the remaining options. Composed of PLA, the Proto-Pasta filament will also help with the structural integrity of the 3D printed battery and provide a rigid surface for the electrodeposition of metal ions. A flexible material, on the other hand, would dislodge and break apart the layer of metal electrodeposition when strained.

Furthermore, to accompany the electrically conductive material, an electrically non-conductive material will need to be used to isolate the 3D printed electrodes within the 3D printed sample. The layer adhesion of the two materials should be optimal to ensure structural integrity and prevent contamination by the electrolyte through possible cracks in the structure. Therefore, the material with the best compatibility with Proto-Pasta would be electrically non-conductive PLA due to their homogeneity.

3.3 3D Printer

3D printers come in all different sizes, mainly depending on the build volume they can accommodate. For the design of the 3D printed battery, it is not recommended to base the entire design on the capabilities of a specific 3D printer as it could limit the reproduction of the design on other printers that lack those specific features. Rather, a more generalized requirement list for the feature set of the 3D printer should be made.

Given the two already chosen materials, one of the requirements for the 3D printer should be a dual extruder. Furthermore, since the two materials are PLA-based, a heated build plate should be required to ensure that the first layer adheres to the printer bed and does not rapidly cool down compared to the rest of the print.

With this requirement list, it is possible to move onto the design choices that are impacted by the decisions made inside the 3D printer slicer program.

3.4 Resistivity of Electrode

As mentioned earlier, the 3D printing settings and geometry of the model have an effect on the electrical resistivity of the 3D printed object. Therefore, it is necessary to figure out the orientation of the model that produces the lowest values for electrical resistance.

In terms of Proto-Pasta, the manufacturers themselves have posted claims on their website about the supposed volume resistivity of 3D printed parts; a volume resistivity of $30\,\Omega\,\mathrm{cm}^{-1}$ is experienced in the layers along the x- and y-axes while a volume resistivity of $115\,\Omega\,\mathrm{cm}^{-1}$ is experienced inbetween the layers along the y-axis [pro, 2017]. Also, a number of research papers have concluded that the z-direction in 3D prints have the highest resistivity [Dijkshoorn et al., 2019, Schouten, 2017].

Therefore, for the lowest electrical resistivity, the electrode should be printed horizontally on the build plate of the 3D printer. Furthermore, there is a limit to the vertical thickness of the electrode as the Proto-Pasta filament was shown to permit noticeable deposition of copper up until a distance of 2 mm from the electrical contact point [Kim et al., 2019].

3.5 Electrode Configuration

As determined in the previous section, the electrode should be printed horizontally as the 3D printed lines in the x- and y- direction have a lower electrical resistance than the 3D printed lines in the z-direction. To maximize the amount of metal ions that can be electroplated onto the electrode, the electrode should have a large surface area in the x- and y-direction while maintaining a small thickness in the z-direction. As a result, the final design of each electrode is a plate with a thickness of 0.6 mm, which is the smallest thickness recommended.

As mentioned in Chapter 2, there needs to be an external part of the electrically conductive electrode that is not in contact with the electroplating solution during electrodeposition. The solution is to have the electrodes on the surface of the electrolyte with one of the large sides touching the electrolyte and the other large side protruding out of the electrolyte. Thus, the current carrying wire can be connected to the side that is protruding outwards.

Furthermore, since the two electrodes will be positioned horizontally on the surface of the electrolyte, the 3D printed sample will need to be able to stand on its own, especially outside of laboratory conditions. Thus, by taking all the considerations into account and the fact that placing the electrodes closer together produces a higher current, the final model in Figure 3.1 was made [Guy, 2004].

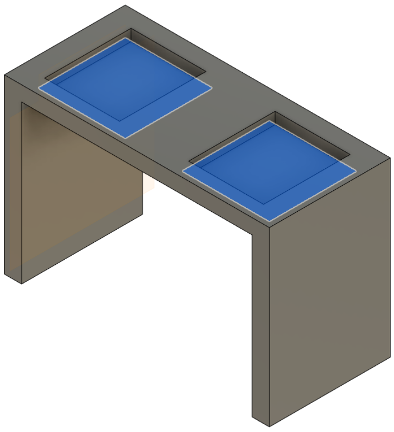

Figure 3.1: A picture of the final 3D battery model in AutoDesk Fusion 360

Moreover, the 3D printed part containing the electrodes has to fit within a standard issue laboratory glass beaker. Standard 1000 mL glass beakers have a diameter of 91 mm [Wikipedia contributors, 2019a]. Thus, the upper limit of the length and width of the 3D printed part is 91 mm; however, given the fact that the copper and zinc cathode still have to fit as well as the reference electrode, this physical limit is much lower.

With the model of the 3D printed battery finalized, it is important to decide upon the choice of electrolyte.

3.6 Choice of Electrolyte

Apart from the sulfuric acid in Figure 2.1, the electrolytes that are generally used in such applications are weak acids, like citric, acetic, and phosphoric acid, due to their relative abundance and low health hazard [Guy, 2004]. They all contain hydrogen ions that are necessary for the redox reactions.

As has been proven, zinc generally dissolves more easily in stronger acids and achieves the highest voltage potential with sulfuric acid as the electrolyte [Guy, 2004]. The Nernst equation predicts that the voltage of a cell is dependent upon the acidity of the electrolyte; therefore, as the pH level increases, the cell voltage decreases [Wikipedia contributors, 2019h].

Thus, sulfuric acid would be the preferred choice as the electrolyte of the 3D printed battery with a pH level of 0.3. However, the end use case for the 3D printed battery would be to utilize the battery as a demonstration of the potential of electrodeposition. Therefore, the 3D printed battery should be safe to operate outside lab conditions and not contain any hazardous materials.

As mentioned at the start of this chapter, the final concept of the 3D printed battery will consist of an open air beaker that will house the electrolyte. Since sulfuric acid is corrosive and produces toxic fumes, another choice for the electrolyte should be considered. Thus, the decision was made to use citric acid with a pH level of 2.2 as the electrolyte for the battery as it is safe to use with one's hands, does not require extreme care when disposing, and is readily available in most cases. In the case of the lemon battery, the maximum voltage that can be achieved is 0.9 V [Wikipedia contributors, 2019h].

3.6.1 Issue with Electrolysis of Solution

During the review of the electrolytes in the previous section, one issue that should be considered is the electrolysis of the electrolyte. Citric acid solution contains citric acid and distilled water, which splits at a potential difference of 1.23V [Wikipedia contributors, 2019d]. The electrolysis of water should not be an issue as the cell voltage should not exceed 0.9V.

In the following chapter, the charactirzartion methods will be presented.

4 Characterization

In this chapter, an overview will be provided about the different measurement methods that will used to characterize the electrodeposition process as well as model the different components of the 3D printed battery. In addition, the methods used to characterize the 3D printed battery as a whole will be given.

4.1 Structural Analysis

Apart from a small segment on the 3D printing process, the structural analysis of the 3D printed battery will mainly focus on the verification of the amount of copper and zinc deposited during the electrodeposition process. The current and voltage measurements will be taken by the Galvanostat and used to mathematically calculate the amount of metal ions deposited. To further verify the effectiveness of the electrodeposition process, the weighting of the 3D printed sample will also be conducted.

The measured results will be compared with the expected results.

4.2 Electrochemical Impedance Analysis

Electrochemical impedance analysis allows for the understanding of how the 3D printed battery operates in different scenarios by identifying the dielectric and electric properties of individual contributions of the components within the battery [ele, 2019, Ramasamy, 2013, Shih and Lo, 1996]. More specifically, electrochemical impedance analysis uses a device called the LCR meter to measure the inductance (L), the capacitance (C), and the resistance (R) of the electric device in question [Ramasamy, 2013]. Also, EIS is a non-invasive method that can be applied to active batteries [Shih and Lo, 1996].

With the values of the impedance of the battery, EIS uses electrical circuits built from components such as resistors and capacitors to model the behavior [Ramasamy, 2013]. The most commonly used electric circuit in EIS is called the Randles circuit, which consists of an active electrolyte resistance in series with the parallel combination of a double-layer capacitance and a charge transfer resistance [ele, 2019, Ramasamy, 2013, Shih and Lo, 1996].

The Randles circuit can be seen in the top left of Figure 4.1 along with an example of the corresponding Cole-Cole plot made from data from a LCR meter.

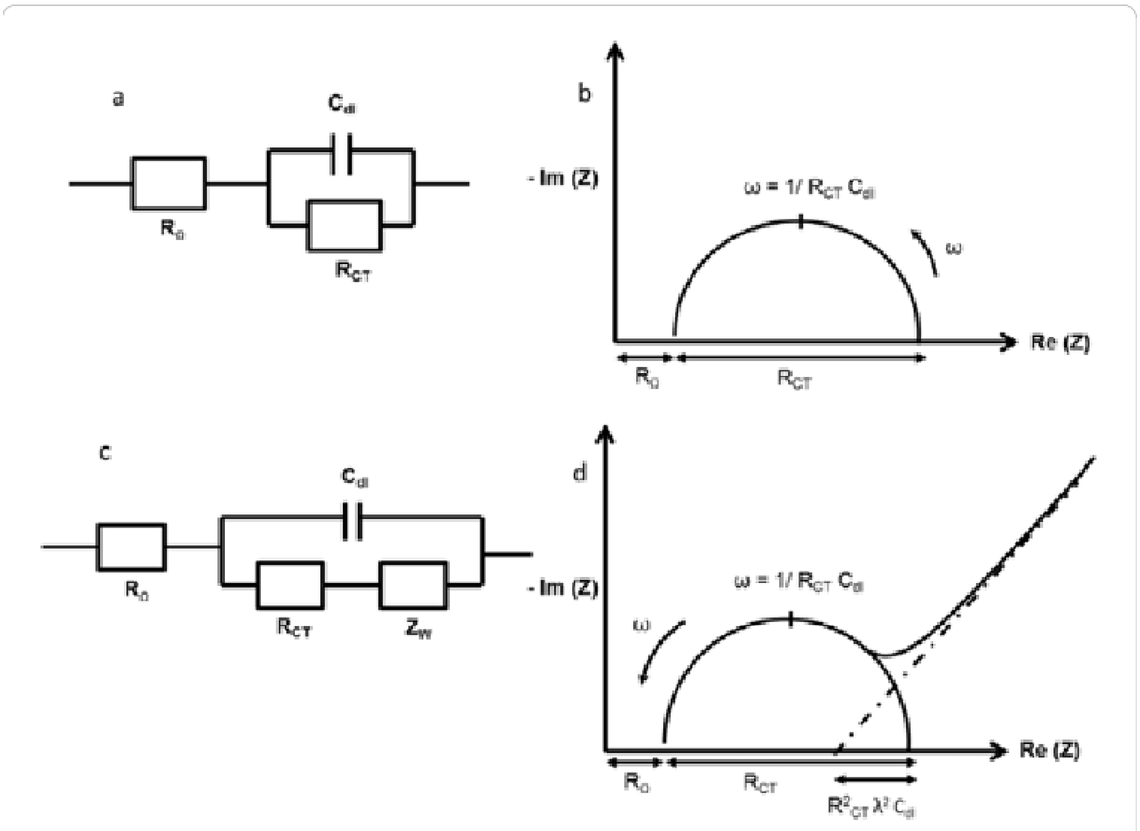

Figure 4.1: Two Cole-Cole plots and their corresponding equivalent electronic circuits, or Randles models [ele, 2019]

As can be seen in Figure 4.1, active electrolyte resistance is found by looking at the x-intercept of the curve on the Cole-Cole plot [ele, 2019]. Furthermore, the charge transfer resistance is found by calculating the distance inbetween the two x-intercept values of the curve [ele, 2019]. Therefore, by measuring the 3D printed battery with the LCR meter, a Randles model of the 3D printed battery can be made.

4.3 Discharge Test

In terms of batteries, the most useful specification for commercial users is the rated capacity. With the rated capacity, the user can make the determination whether the battery can supply the adequate amount of current for the intended period of time. Therefore, the 3D printed battery must be discharged to determine its capacity.

The capacity of the battery as well as other characteristics can be seen from the graph of the discharge cycle of the battery. Generally, for the discharge cycle of a battery, the voltage of the battery versus time is plotted separately from the current of the battery versus time. However, many research papers plot the voltage of the battery over the specific capacity of the battery as can be seen in Figure 4.2 and 4.3.

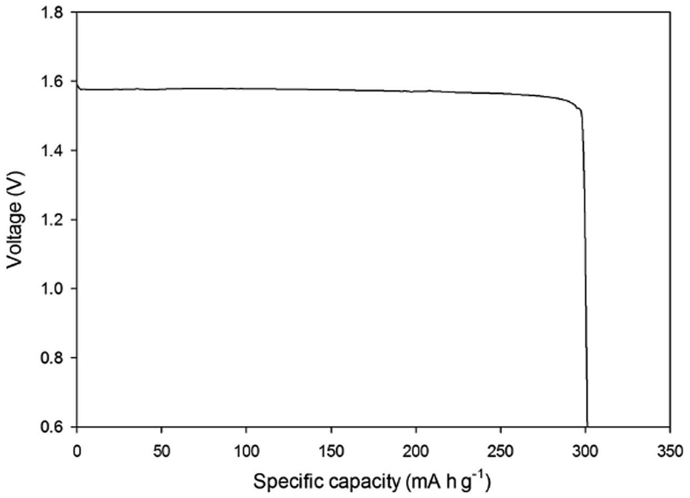

Figure 4.2: A graph of the discharge cycle of a zinc-carbon battery with units of voltage over units of specific capacity [Alias and Mohamad, 2015]

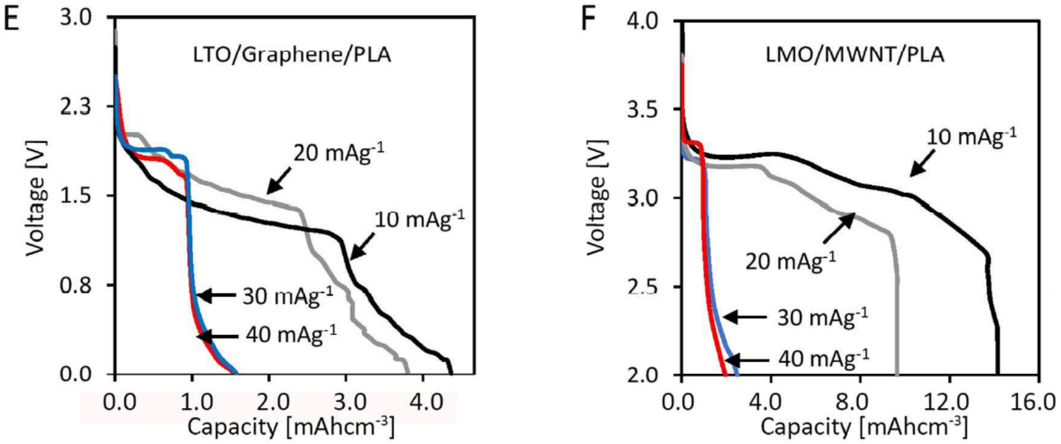

Figure 4.3: Two graphs of the discharge of a lithium titanium oxide and lithium manganese oxide batteries with units of voltage over units of specific capacity at different discharge currents [Reyes et al., 2018]

Glancing at the graph in Figure 4.2, several of the characteristics of batteries can be pointed out. The initial voltage, also the highest value on the curve, is the maximum voltage that the battery can deliver and therefore, is called the maximum theoretical voltage if all the components are ideal [Wikipedia contributors, 2019c]. However, as one can see, the maximum voltage is not sustained for the majority of the life cycle of the battery; instead, the voltage drops and a plateau is observed and centers around one value, which is called the nominal practical voltage. The nominal practical voltage is the voltage that the user of the battery can expect to observe at the output.

Specific energy of the battery, on the other hand, defines the battery capacity in relation to weight as can be seen on the axes of the graphs in Figure 4.2 and 4.3. To calculate the capacity of the battery, it requires taking either the integral of the area under the curve of the voltage graph over time multiplied with the inverse of the value of the resistor or simply taking the integral of the area under the curve of the current graph over time. With the value of the current over the set time period, the capacity of the battery can be expressed as Ah.

Thus, the rated capacity of the 3D printed battery of this thesis will be calculated from the integral of the current over time and compared to the capacity of other batteries such as the ones in Figure 4.2 and 4.3.

In the next section, the methodology of the 3D printed battery will be given.

5 Method

This chapter discusses the fabrication of the 3D printed battery and the processes and measurement setups that arise from its creation. In the first section, the 3D printer settings will be mentioned in great detail as it is known that they have a significant impact on the electrical resistivity of the finished 3D print [Zhang et al., 2017c]. Afterwards, the specifics of the electrodeposition process will be presented, particularly the composition of the baths and currents applied to the electrodes, and followed by the final implementation of the 3D printed battery, chiefly the preparation and containment of the electrolyte. Lastly, the measurement setups that were used to carry out the characterization of the 3D printed battery as described in chapter 4 will be mentioned.

Before the immersion into the electrolyte, the 3D printed battery is referred to as the 3D printed sample in the following chapters.

5.1 3D Printing

As can be seen in Figure 5.1, the model in Figure 3.1 consists of three separate models; two individual models for the right and left electrodes and one individual model for the housing of the electrodes. The dimensions of the 3D printed sample can be seen in Appendix B in Figure B.1, B.2, and B.3. As can be seen in Figure B.2, the length and width of the electrodes is set to 15 mm and the thickness is set to 0.6 mm. Furthermore, as can be seen in Figure 5.1, additional extrusions were added in the cutouts for further support of the thin electrodes during the 3D printing process.

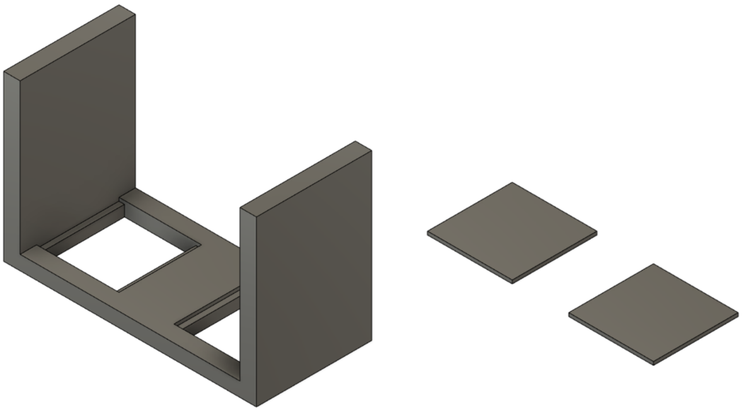

Figure 5.1: A picture of the individual Autodesk Fusion 360 models of the electrodes and housing

The three STL models from AutoDesk Fusion 360 were combined and sliced with Simplify3D. The two electrodes were 3D printed from rigid carbon black filled PLA (Proto-Pasta [pro, 2017]) and the housing was 3D printed from rigid blue colored PLA using the FlashForge Creator Pro with the Flexion dual extruder [FlashForge, 2017]. Furthermore, the build plate was manually leveled by turning the three knobs on the underside of the build plate.

To ensure proper first layer adhesion as well as easy removal of the finished 3D print afterwards, kapton tape was applied across the length of the build plate. Also, as the build plate was heating up to the desired temperature of 60 °C, 3DLAC spray adhesive was sprayed onto the area of the kapton tape where the filament would be deposited.

In regards to the Simplify3D parameters, the settings for both the normal and electrically conductive PLA were set to the following:

Table 5.1: Table of the 3D printer settings for electrically non-conductive PLA and electrically conductive Proto-Pasta PLA

	PLA	Proto-Pasta PLA
Printing Temperature	205 °C	220 °C
Extrusion Multiplier	1.20	1.30
Extrusion Width	0.4 mm	0.4 mm
Layer Height	0.2 mm	0.2 mm
Infill(%)	100	100
Prime Pillar	Enabled	Enabled
Skirt	Enabled	Disabled
Support	Disabled	Enabled
Retraction	Enabled	Enabled

Furthermore, the extrusion multiplier was set above 100 for both materials to ensure that there were no gaps in-between the electrodes and the housing that would otherwise ruin the 3D print during the electrodeposition process by allowing the electroplating solution to seep through. Likewise, prime pillars and a skirt were utilized to avoid cross-contamination of the different materials during the 3D printing process. In Simplify3D, the model was placed upside down to minimize the amount of support needed and to have the electrodes printed horizontally in accordion with the decision made in Chapter 3.

Once the 3D printing had finished, the 3D printed sample was removed from the build plate with the use of ethanol as to not damage the print through the conventional scraping method.

5.2 Issue with Wiring the 3D Printed Battery

To prepare the 3D printed sample for the electrodeposition process and the final battery stage, a wire was attached to the top-side of each electrode. Due to the melting temperature of PLA, a soldering iron could not be used to solder the wires onto the 3D printed electrodes. Instead, Electrolube silver conductive paint was applied along the entire surface area of the top-side of both 3D printed electrodes to ensure that the current from the wire was uniformly spread throughout. Then, the current carrying wires were placed on top of the silver painted areas and secured in place with strips of electrical tape.

5.3 Electrodeposition

Once the 3D printing had been completed, the 3D printed sample was subjected to the electrodeposition process.

The 3D printed sample was first submerged into a 250 mL beaker of ethanol and placed into an ultrasonic bath for 60 s to increase the surface wettability and clean the surfaces before the insertion into the electroplating solution [Kim et al., 2019]. Then, once the 3D printed sample had been dried, the conductive silver paint was applied to the top-side surfaces of the electrodes. Afterwards, as illustrated in Chapter 2, the three electrode setup with the Galvanostat was assembled, which was followed by the preparation of the copper and zinc bath solutions. Next, the 3D printed sample was inserted into each bath solution and electroplated with each metal. The following sections describe the electrodeposition process in further detail.

All the materials and equipment utilized were specifically chosen for the purpose of being used in standard laboratory beakers.

5.3.1 Three Electrode Setup

Except for the cathode and electroplating solution, the same equipment was used for the electrodeposition of copper and zinc. To drive the chemical reaction of reduction, the Keithley 2410 power supply with four-wire sense was used [Keithley, 2014].

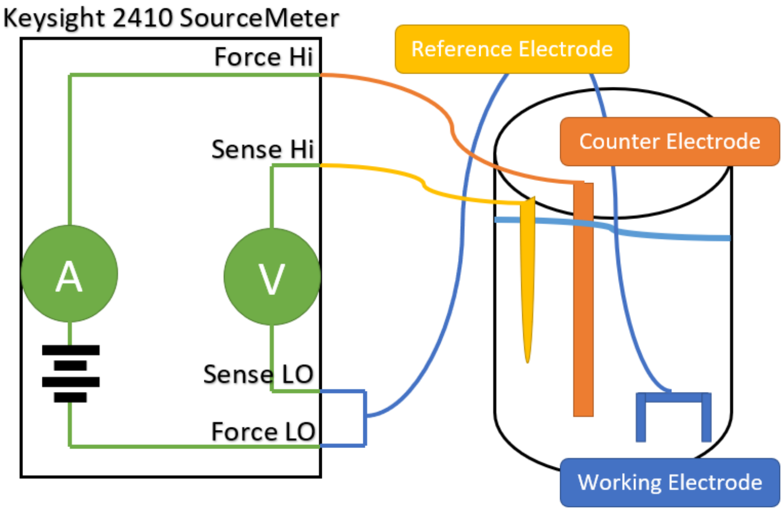

Figure 5.2: A diagram of the three electrode setup sued for the electrodeposition process

As can be seen in Figure 5.2, the Force-HI port of the power supply was connected to the counter electrode, or cathode. The Sense-Hi port of the power supply was connected to the reference electrode and the Force-Lo and Sense-Lo were connected to the working electrode, or anode. The material of the counter electrode was dependent on the metal that was to be electrodeposited. In the case of the copper electrodeposition, a copper cathode of 99.99% purity that measured 5 cm by 10 cm was used. A zinc cathode of 99.99% purity that measured 5 cm by 8 cm was used for the zinc electrodeposition. A general rule of thumb is that the surface area of the counter electrode should be ten times greater than that of the working electrode. Likewise, for the electrodeposition of each metal, the wire connecting the working electrode, or the 3D printed sample, to the power supply was switched from one electrode on the 3D printed sample to the other. In both cases, the reference electrode was a silver-chloride electrode.

Pictures of the configuration of the electrodes for each electrodeposition process can be seen in Figure 5.3 and 5.4. As can be seen in Figure 5.3 and 5.4, the reference electrode is positioned behind the counter electrode as it should never be in the electric field lines between the counter and working electrodes. Otherwise, the counter electrode would measure a voltage drop.

Each electrodeposition run was conducted for a duration of approximately 30 min as there was no significant drop in the electrical resistance of the 3D printed Proto-Pasta electrode from 30 min to 60 min at a distance of 1 cm from the electrical contact point [Kim et al., 2019].

5.3.2 Copper Electrodeposition

The following section concerns with the details specific to copper electrodeposition. The composition of the copper electroplating solution follows the research work done by another paper; originally intended to create enough electroplating solution for a 10 L bath, the procedure consists of the following steps [Bart, 2009]:

1. Fill 7 L DI water into the tank
2. Add 0.3 L Sulfuric Acid (H_2SO_4) with constant stirring

3. Mix well
4. Add 1 kg Copper Salt FG and dissolve
5. Add 0.8 L Sulfuric Acid (H_2SO_4) with constant stirring
6. Mix well
7. Add 2 mL Hydrocloric Acid (HCL)
8. Add 0.1 L Slotocoup HL11
9. Add 3 mL Slotocoup HL13
10. Mix well
11. Make up to final volume with DI water
12. Mix thoroughly

As can be noticed above, the procedure contains a few additives that are intended to accelerate the electroplating process. To ensure that the surface of the anode is uniformly electroplated, the copper bath was stirred using a magnetic stirrer at a speed of 300 RPM to circulate the supply of copper ions [Kim et al., 2019]. Additionally, the underside of the electrode that is to be electroplated is pre-wetted with the copper electroplating solution to expel any air bubbles.

Given the surface area of the 3D printed electrode to be 2.25 cm^2 and the current density of 3 mA/cm^2, the current source of the power supply was set to 6.75 mA [Kim et al., 2019].

The final copper electrodeposition setup can be seen in Figure 5.3. The beaker was filled with the copper electroplating solution until the underside of the 3D printed sample was submerged.

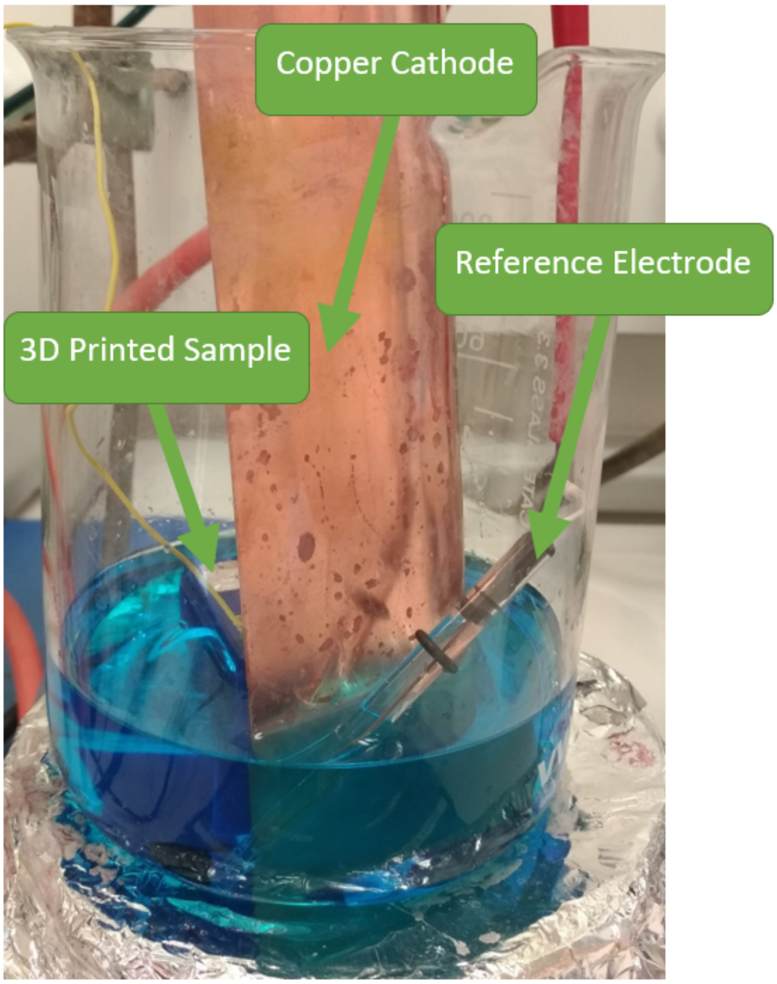

Figure 5.3: A picture of the copper electrodeposition setup with labels for the three electrodes

5.3.3 Zinc Electrodeposition

This section deals with the particulars of zinc electrodeposition. Unlike the complex procedure to formulate the copper electroplating solution, the process to create the zinc electroplating solution involves only one chemical solution: zinc sulfate. Therefore, 1.0 mol of zinc sulfate solution was poured into the beaker until the underside of the 3D printed sample was submerged.

Once again, to ensure that the surface of the anode is uniformly electroplated, the zinc bath was stirred by a magnetic stirrer at a speed of 100 RPM to circulate the supply of zinc ions [Alias and Mohamad, 2015]. The underside of the electrode was pre-wetted with the zinc electroplating solution.

Given the surface area of the 3D printed electrode to be 2.25 cm^2 and the current density of 20 $\mathrm{mA/cm}^2$, the current source of the power supply was set to 45 mA [Alias and Mohamad, 2015].

The final configuration of the electrodes can be seen in Figure 5.4.

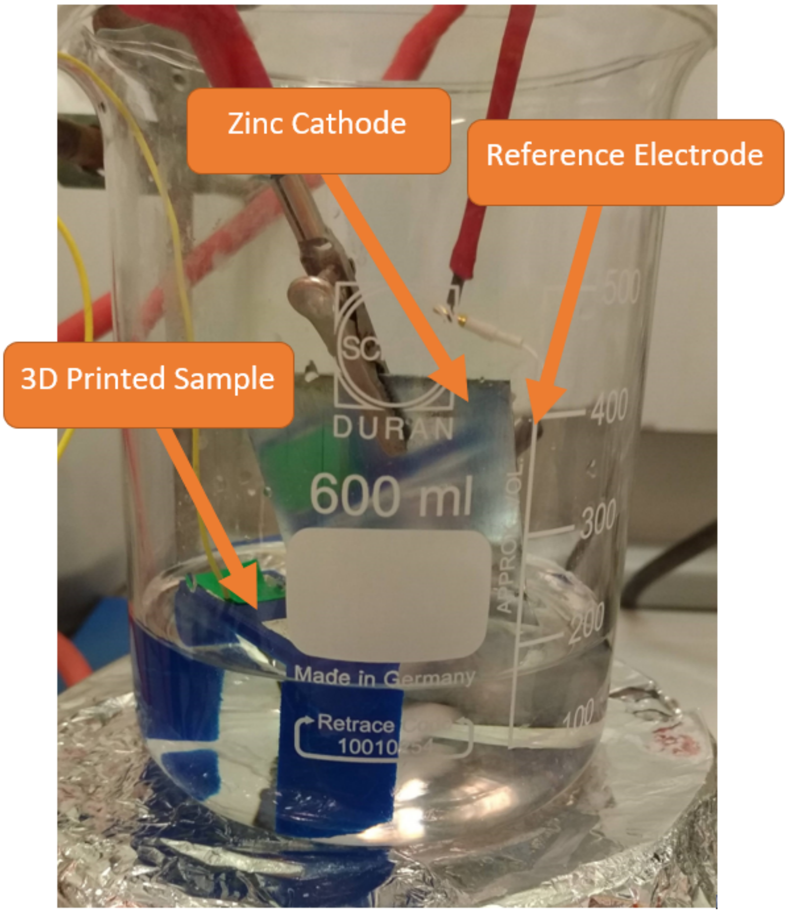

Figure 5.4: A picture of the zinc electrodeposition setup with labels for the three electrodes

5.3.4 Measurement Setup

Likewise, it is important to obtain the correct measurements during the electrodeposition process for the purpose of evaluation later on.

To measure the amount of metal electrodeposited during the two electrodeposition processes, the weighting of the 3D printed sample at different stages was conducted using an electronic scale.The 3D printed sample was measured straight after being 3D printed. Next, it was measured after the Ethanol cleaning bath and weighted after the silver paint has been applied. Then, before the current was applied in each of the electrodeposition processes, it was weighted after being immersed in each of the electroplating solution. Lastly, the 3D printed sample was weighted after the electrodeposition of each metal.

Moreover, during the electrodeposition process, the Galvanostat will measure the voltage and current passing through the entire system of electrodes and electrolyte. Therefore, it is important to configure the power supply to communicate in RS-232 mode so that the Matlab script in Appendix A can be used to set the current and capture the data to be plotted afterwards [Keithley, 2014].

With the weight and Galvanostat measurements, there is redundancy in the collection of data and the cross-examination of the results can be conducted.

5.4 Final Battery Fabrication

Once the 3D printed sample was electroplated, the 3D printed battery was finalized by immersing the electroplated 3D printed sample into the citric acid electrolyte.

Normally, in a laboratory setting, citric acid comes in powder form and requires the addition of boiling water to completely dissolve and become a homogeneous solution. With the molecular mass of citric acid at 192.12 $\mathrm{g\,mol^{-1}}$, 19.212 g of citric acid was combined with 100 mL of boiling water to obtain 100 mL of electrolyte [cit, 2019]. The 100 mL of citric acid electrolyte was then placed inside a 250 mL glass beaker. The size of the beaker will determine the quantity of electrolyte that needs to be made as the glass beaker should be filled up until the underside of the 3D printed sample is submerged. The final result can be seen in Figure 5.5.

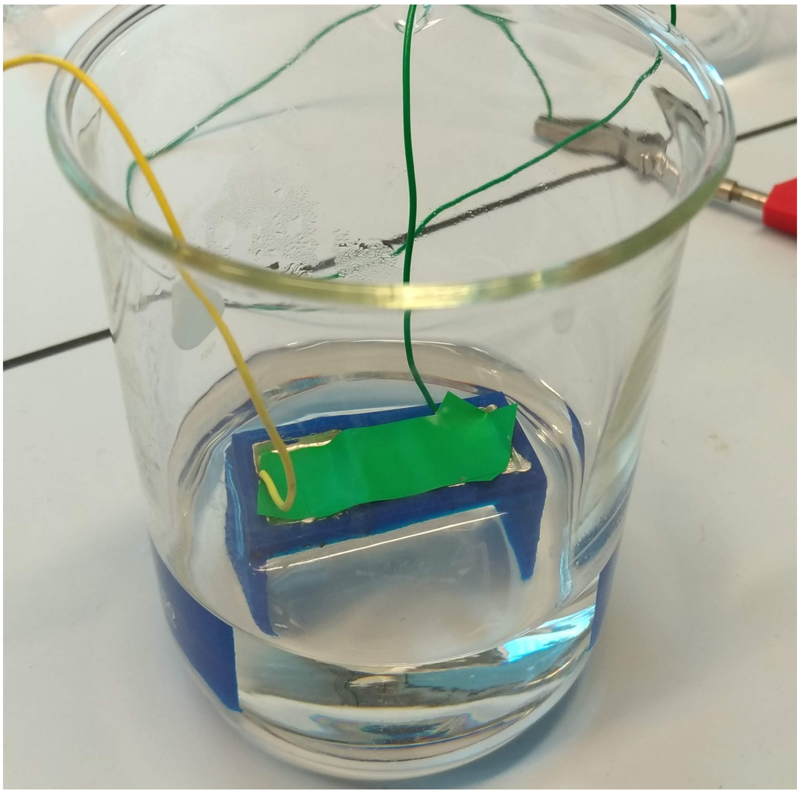

Figure 5.5: A picture of the final product with the electroplated 3D printed sample immersed in the citric acid electrolyte with the wires connected to the plus and minus terminals

5.4.1 Measurement Setup

Similarly, like in the measurement setup for electrodeposition, it is vital to have the proper equipment to conduct the characterization methods outlined in chapter 4.

For the LCR measurements, the LCR meter used was the HP 4284A Precision LCR Meter with a frequency range of 20 Hz to 1 MHz. As can be seen in Appendix A, Matlab code was used to program the LCR meter and set the specific frequencies for the LCR measurements; the LCR meter was configured to perform two frequency sweeps on the set of frequencies shown in Figure 5.6. The LCR meter measured the magnitude and phase of the impedance.

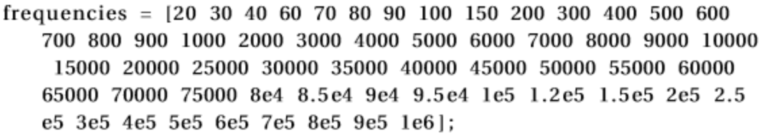

```
frequencies = [20 30 40 60 70 80 90 100 150 200 300 400 500 600
    700 800 900 1000 2000 3000 4000 5000 6000 7000 8000 9000 10000
     15000 20000 25000 30000 35000 40000 45000 50000 55000 60000
    65000 70000 75000 8e4 8.5e4 9e4 9.5e4 1e5 1.2e5 1.5e5 2e5 2.5
    e5 3e5 4e5 5e5 6e5 7e5 8e5 9e5 1e6];
```

Figure 5.6: A screenshot of the set of frequencies used for the LCR measurements

Using the four-wire sense of the LCR meter, the lowside-current and -voltage wires were attached to the zinc electrode and the highside-current and -voltage wires were connected to the copper electrode. The electroplated 3D printed sample was immersed in the electrolyte as shown in Figure 5.5 for the LCR measurements.

For the discharge measurements of the 3D printed battery, the Keysight 34461A Digital Multimeter was used [Keysight, 2019]. As mentioned in Chapter 4, the capacity of the battery is measured in units of ampere-hour, or Ah. Therefore, the multimeter measured the output current from the 3D printed battery over time as it was discharged through an external load. To easily obtain the values of the voltage from the current measurements, a load of 1 Ω was placed in series with the 3D printed battery.

Once the redox reactions had ceased, the 3D printed sample was removed from the depleted citric acid electrolyte, electrodeposited with zinc again, and placed in a new solution of citric acid to start over with the measurements.

In the following chapter, the results obtained from the measurement setups will be discussed.

6 Results and Discussion

In this chapter, the measurement results from the different measurement methods presented in Chapter 4 will be given. The measurement data from the electrodeposition process is compared to the theoretical calculations. Likewise, the LCR measurements are presented and analyzed to provide a representative model of the battery. Lastly, the current and voltage measurements of the discharge cycle of the battery are shown and interpreted to determine the capacity of the battery.

The measurement methods were performed in the manner as described in their corresponding chapters.

6.1 Structural Analysis

Before the results of the electrodeposition are given, a brief section on the challenges encountered during the 3D printing process will be given.

6.1.1 3D Printing

Several adjustments were made to the printing parameters and the model for the 3D printed battery went through a few iterations after some trial-and-error. One of the more significant changes to the printing parameters was the initial layer height. When the Proto-Pasta was printed directly onto the build plate, the first layer had the tendency to stick to the build plate and rip itself off the rest of the 3D printed sample when it was removed after completion. This was a major issue with the first iteration of the 3D printed sample as can be seen in Figure 6.1a and 6.1b as the thickness of the main structure was only 2 mm. Thus, the initial layer height of the Proto-Pasta was set to 0.3 mm to ensure that the first layer of the Proto-Pasta came off the build plate with the rest of the 3D print. Later on, when walls were added to the top side of the 3D printed sample as can be seen in the second iteration in Figure 6.2a and 6.2b, supports had to be enabled under the entire Proto-Pasta section and the issue with the Proto-Pasta sticking was completely avoided. In addition, prime pillars were initially used, but were disabled in the final iteration when the dual extruder setup kept knocking them over. Instead, the retraction distance was increased from 6 mm to 12 mm. Lastly, leveling the build plate was the single most significant contributor to the success of the 3D print.

The first iteration of the 3D printed sample can be seen in Figure 6.1a and 6.1b.

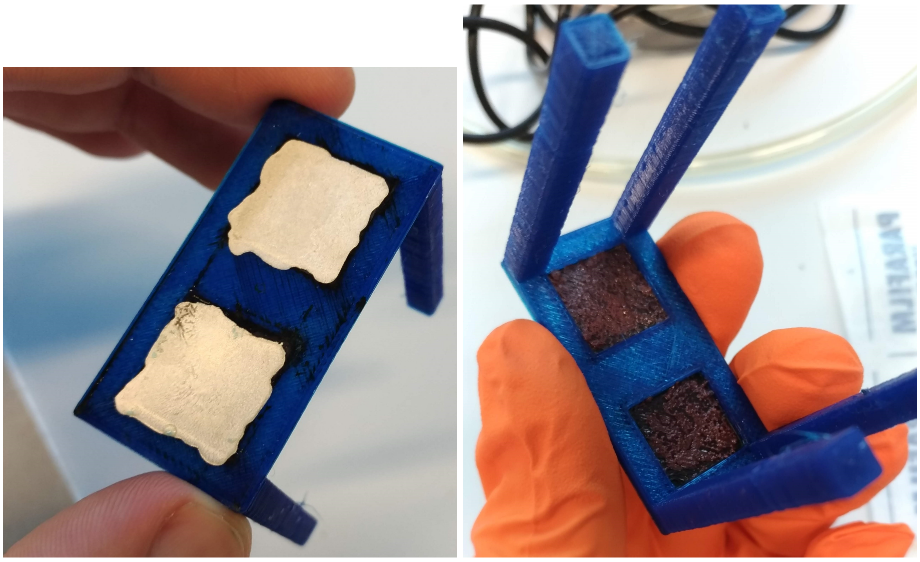

(a) A top view picture of the first iteration of the 3D printed sample **(b)** A bottom view picture of the first iteration of the 3D printed sample

Figure 6.1: Pictures of the first iteration of the 3D printed sample

The first iteration was 3D printed in the up-down orientation as can be seen in Figure 6.1b. Most of the 3D prints had to be discarded before completion as the four thin legs had a huge risk of being knocked over by the extruder during the printing process. In addition, the lack of walls along the top side of the 3D printed sample meant that the slightest ripple in the electroplating solution would easily overcome the small height difference and contaminate the entire 3D print during the electrodeposition process.

The next iteration as can be seen in Figure 6.2a and 6.2b included raised walls and replaced the four slender legs for two larger ones instead. The model in the figures had a height of 25 mm that posed a nuisance during the electrodeposition process as it was quite challenging to lower and remove from the glass beaker.

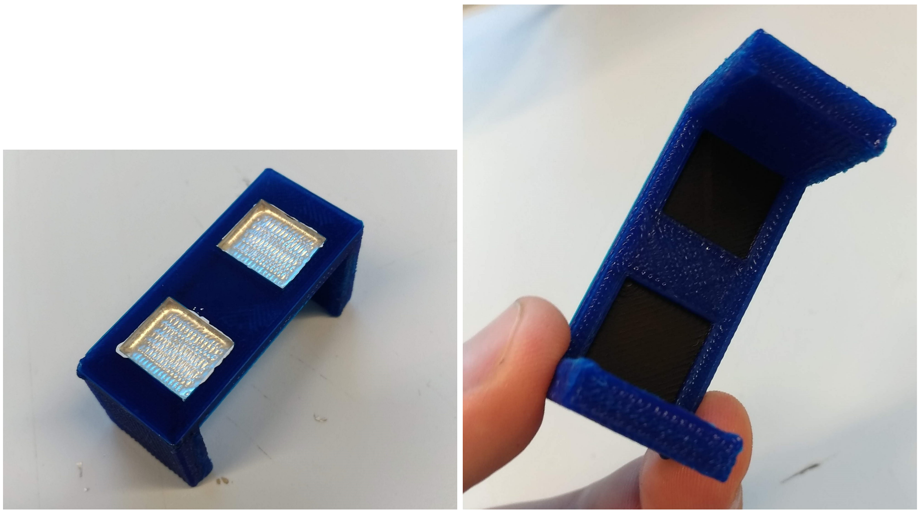

(a) A top view picture of the second iteration of the 3D printed sample **(b)** A bottom view picture of the second iteration of the 3D printed sample

Figure 6.2: Pictures of the second iteration of the 3D printed sample

With these issues in mind, the final model in Figure 3.1 was made 5 mm higher and the two legs were shortened in width by 0.5 mm to keep the printing time under two hours.

6.1.2 Issues with the Wiring of the 3D Printed Sample

Moreover, issues arose when the electrical tape holding the wires would tear themselves from the surface of the electrode when presented with an aqueous solution such as the electroplating solution. The problem was simply fixed through the drying of the surface and the application of an external force on the electrical tape.

The possibility of using epoxy to permanently glue the wires to the electrodes was considered. However, it was decided that the presence of the wires would interfere with the weight measurements intended to measure the amount of metal deposited during the electrodeposition process.

6.1.3 Electrodeposition

During the process of electrodeposition, the Galvanostat with its three electrode setup was used to obtain the data in Figure 6.3, 6.4, 6.5, and 6.6.

6.1.4 Copper Electrodeposition Results

Irrespective of the order of electrodeposition, the copper electrodeposition was the first metal to be electroplated in this case. The graphs of the current and voltage measurements during the electrodeposition process can be seen in Figure 6.3 and 6.4.

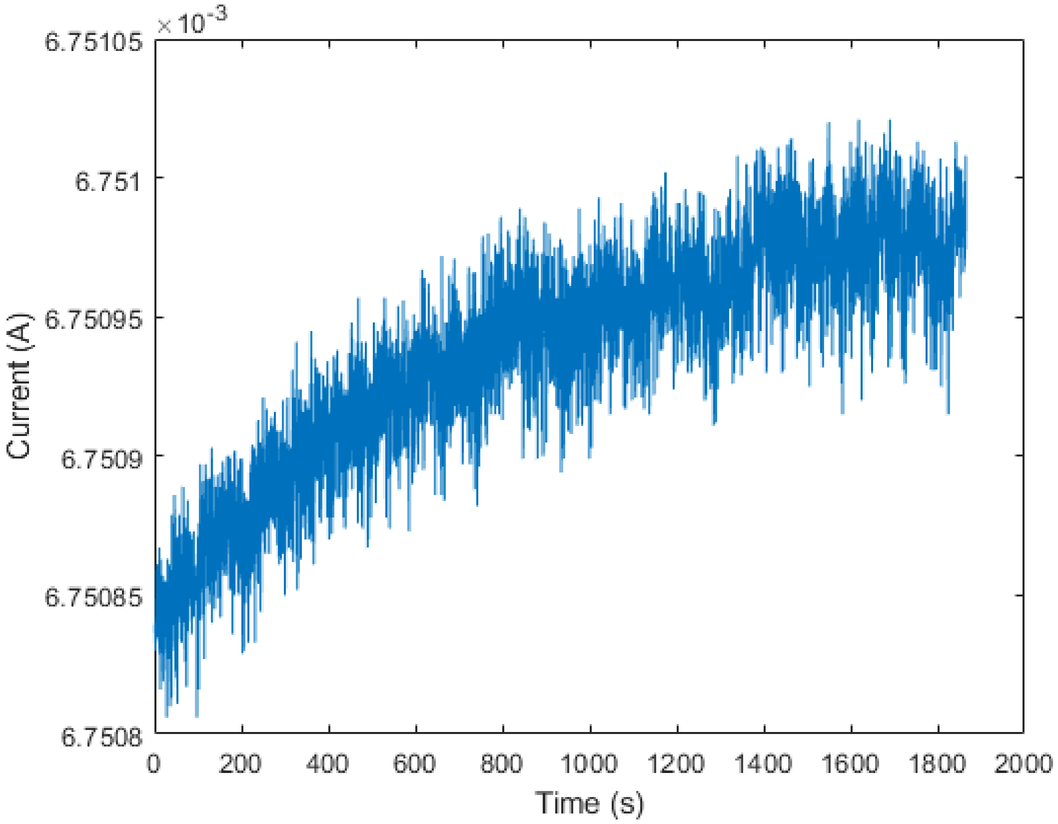

Figure 6.3: A graph of the current vs. time of the copper electrodeposition

As can be seen in Figure 6.3, the current value of 6.75 mA that was specified in Chapter 5 was achieved with a visible upwards trend. The slight upwards trend of the current can be attributed to the decrease of the electrical resistance of the electrode over time due to the constant deposition of copper onto the electrode. Using Faraday's Law of Electrolysis, the amount in grams of the copper that was electrodeposited can be calculated for the theoretical current of 6.75 mA and the measured current as follows:

$$Q_{Theoretical} = \int_0^T I dt = (6.75\,\mathrm{mA}) \cdot (1864.6\,\mathrm{s}) = 12.586\,05\,\mathrm{C} \tag{6.1}$$

$$Q_{Measured} = \int_0^T I dt = \int_0^{1864.6} I dt = 15.68\,\mathrm{C} \tag{6.2}$$

$$m_{theoretical} = \frac{M \cdot Q}{z \cdot F} = \frac{63.546\,\mathrm{g\,mol^{-1}} \cdot 12.586\,05\,\mathrm{C}}{2 \cdot 96\,485.332\,89\,\mathrm{C\,mol^{-1}}} = 0.004\,14\,\mathrm{g} \tag{6.3}$$

$$m_{measured} = \frac{M \cdot Q}{z \cdot F} = \frac{63.546\,\mathrm{g\,mol^{-1}} \cdot 15.68\,\mathrm{C}}{2 \cdot 96\,485.332\,89\,\mathrm{C\,mol^{-1}}} = 0.005\,16\,\mathrm{g} \tag{6.4}$$

Thus, from the calculations above, the amount of copper electrodeposited during the experiment exceeded the theoretical estimate. However, the current measurements are no guarantee that the amount of copper calculated was the amount of copper electrodeposited as there is the possibility that some of the current went towards the electrolysis of the electrolyte. Since no visible bubbles were observed during the electrodeposition process and the fact that the voltage was far below any of the electrolysis values mentioned earlier in this thesis, it was concluded that all the current was dedicated to the electrodeposition of copper.

Likewise, to validate the amount of the copper electrodeposited, weight measurements of the 3D printed sample were taken at various stages during the electrodeposition process; the data can be seen in Table 6.1 and the analysis of the data will be given later on in this section.

Moreover, during the electrodeposition of the copper, the voltage was measured as well. As can be seen in Figure 6.4, the curve follows a bell-shaped, downward trend, which matches expectation; as the copper is deposited, the electrical resistance of the electrode decreases, leading to a lower voltage drop over the material and so forth.

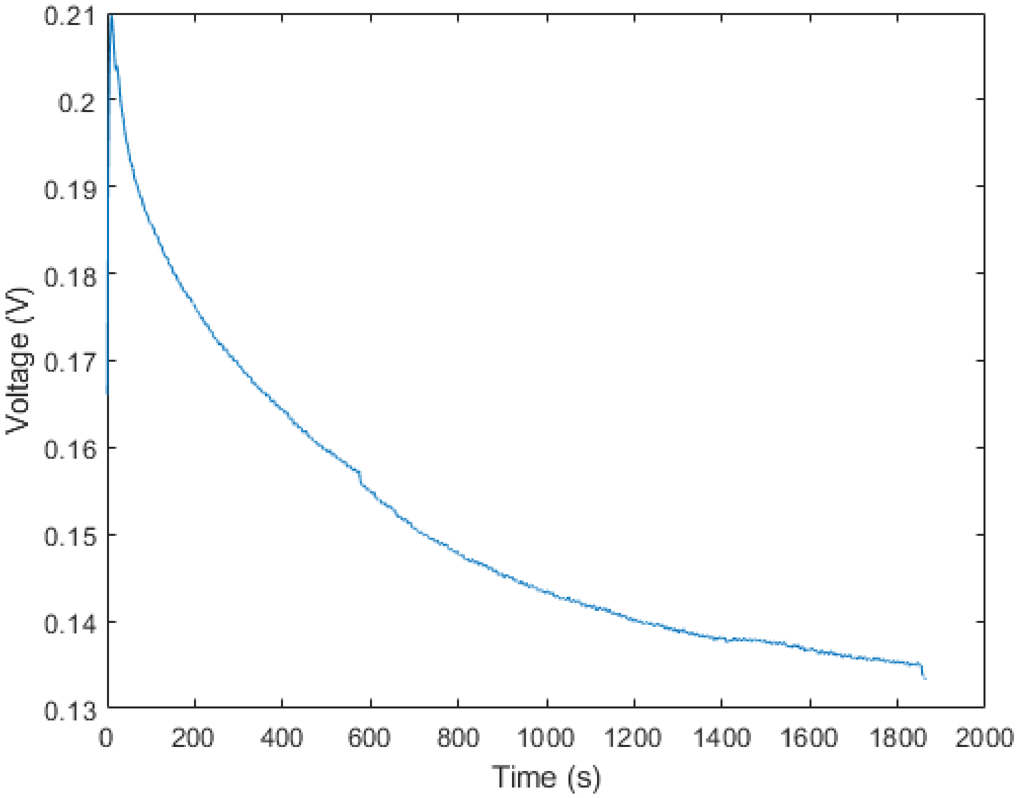

Figure 6.4: A graph of the voltage vs. time of the copper electrodeposition

6.1.5 Zinc Electrodeposition Results

After the copper electrodeposition was successful, the 3D printed sample was subjected to zinc electrodeposition. The graphs of the current and voltage measurements during the electrodeposition process can be seen in Figure 6.5 and 6.6.

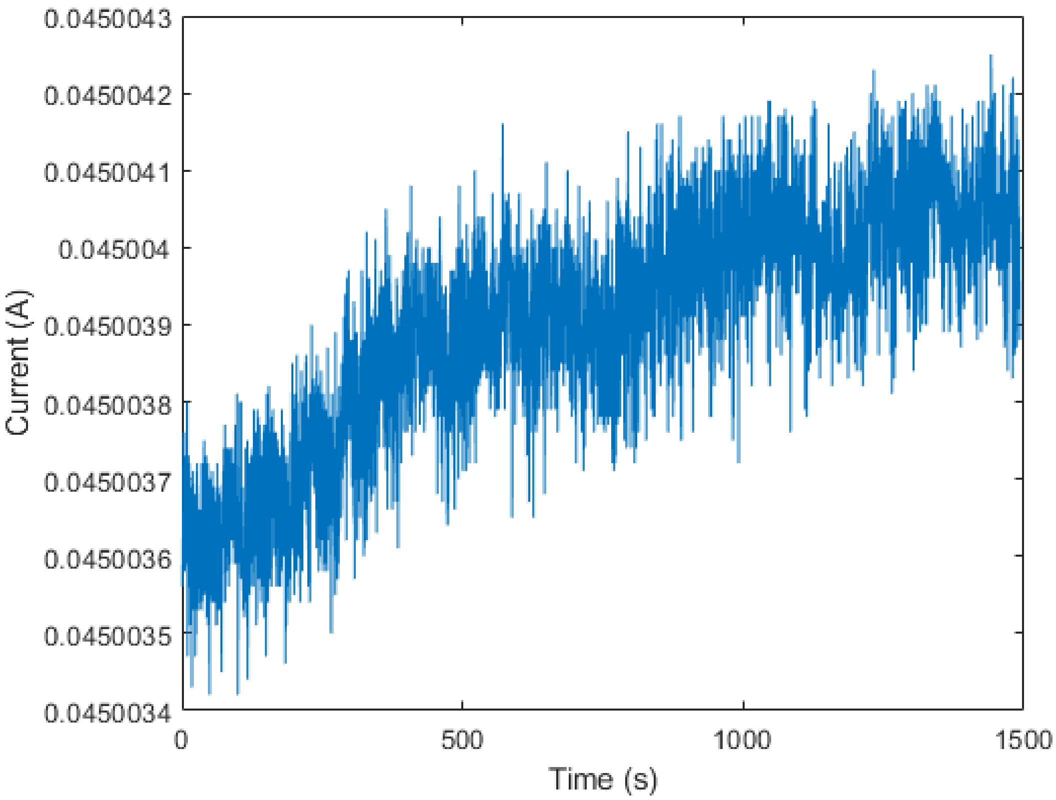

Figure 6.5: A graph of the current vs. time of the zinc electrodeposition

As can be seen in Figure 6.5, the current value of 45 mA that was specified in Chapter 5 was obtained. However, as in the case of the copper electrodeposition, there is a noticeable upward trend in the values of the current. The slight upwards trend of the current can be attributed to the decrease of the electrical resistance of the electrode over time due to the constant deposition of zinc onto the electrode. Using Faraday's Law of Electrolysis, the amount in grams of the zinc that was electrodeposited can be calculated for the theoretical current of 45 mA and the measured current as follows:

$$Q_{Theoretical} = \int_0^T I\,dt = (45\,\text{mA})\cdot() = 67.158\,\text{C} \tag{6.5}$$

$$Q_{Measured} = \int_0^T I\,dt = \int_0^{1864.6} I\,dt = 67.164\,\text{C} \tag{6.6}$$

$$m_{theoretical} = \frac{M\cdot Q}{z\cdot F} = \frac{65.38\,\text{g}\,\text{mol}^{-1}\cdot 67.158\,\text{C}}{2\cdot 96485.33289\,\text{C}\,\text{mol}^{-1}} = 0.02275\,\text{g} \tag{6.7}$$

$$m_{measured} = \frac{M\cdot Q}{z\cdot F} = \frac{65.38\,\text{g}\,\text{mol}^{-1}\cdot 67.164\,\text{C}}{2\cdot 96485.33289\,\text{C}\,\text{mol}^{-1}} = 0.02276\,\text{g} \tag{6.8}$$

Despite the variations in the current, the calculations for the amount of copper deposited in both the theoretical and experimental cases is the approximately the same. Based solely on the calculations of the total charge, the amount of zinc electrodeposition should be approximately 4.3 times the amount of copper electrodeposition. Taking a look at the actual mass calculations, the amount in grams of zinc electrodeposition is 4.41 times the amount of copper electrodeposition.

Visually, as can be seen in Figure 6.7a, the zinc electroplated electrode had a more profound coating than the copper electroplated electrode. However, visual observations are not enough to provide the entire picture.

As mentioned for the copper counterpart, the measured current is not a guarantee that the zinc electrodeposition process has been 100% efficient. But, before any conclusions can be made, it is necessary to look at the graph of the voltage measurements to determine whether the value of the voltage is high enough for electrolysis to occur.

In Figure 6.6, the voltage measurements for the zinc electrodeposition can be seen. The curve initially starts downward and then, shortly slopes upwards before continuing downward at a constant rate. The overall downward trend matches expectation as the increasing deposition of zinc reduces the electrical resistance of the electrode. However, the initial increase in the voltage and the value of the voltage at around 2.35 V is self-evident that the electrolysis of the solution has occurred as sulfate ions undergo electrolysis at approximately 2.010 V. Visual observations of bubbles forming at the electrode further confirms the conclusion.

The formation of oxygen bubbles from the sulfate ions increase the electrical resistance of the material. Then, at some point, the attraction of the zinc ions to the electrode is so great that the zinc ions push out the oxygen gas and deposit themselves onto the surface of the electrode as seen in Figure 6.6 at the peak. To further support this statement, as can be seen in Figure 6.7a, there are small indentations in the zinc deposition on the top electrode that are indicators of the once present oxygen bubbles.

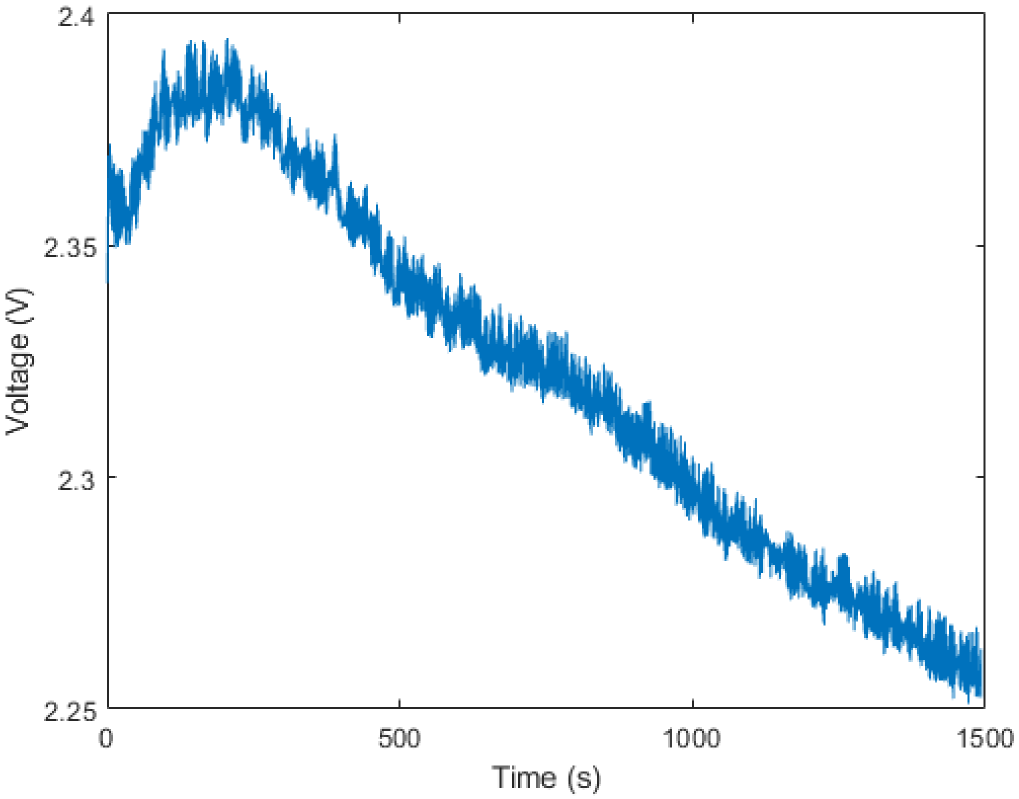

Figure 6.6: A graph of the voltage vs. time of the zinc electrodeposition

A visual of the results of both the copper and zinc electrodeposition can be seen in Figure 6.7a. As can be seen in Figure 6.7a, there is an area on the bottom electrode that is not covered by copper, which resulted from the mishandling of the 3D printed sample during the removal from the copper bath.

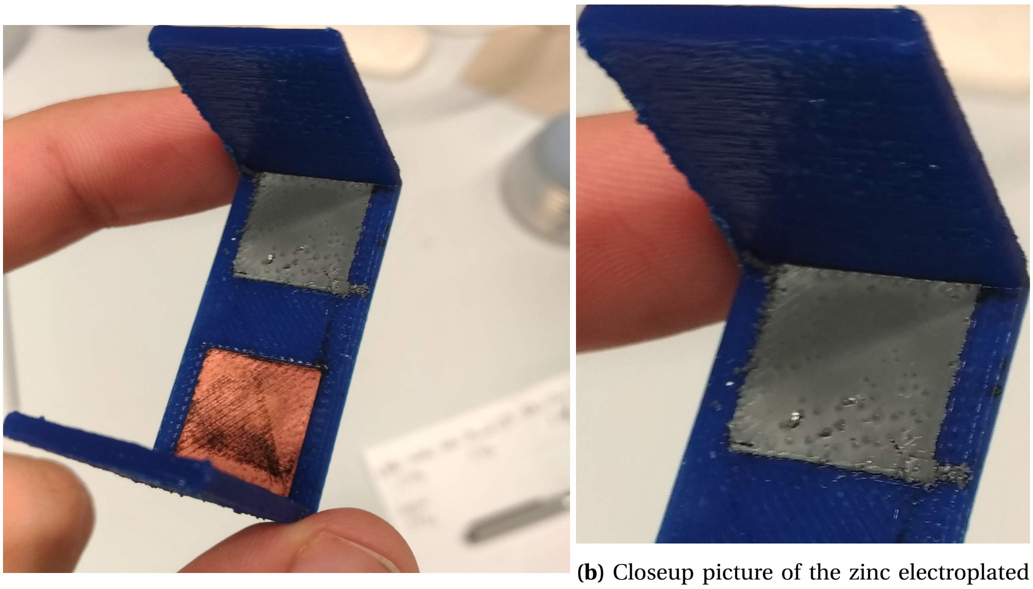

(a) Picture of the copper and zinc electroplated electrodes with noticeable damage to the copper electrode

(b) Closeup picture of the zinc electroplated electrode focusing on the indentations left by the oxygen bubbles

Figure 6.7: A picture of the 3D printed sample after copper and zinc electrodeposition; the magnetic stirrer scratched a portion of copper from the bottom electrode during the removal of the 3D printed sample from the copper bath

Additionally, the weight of the 3D printed sample was taken after the zinc electrodeposition and the measurement can be seen in Table 6.1.

6.1.6 Weight Measurements of Electroplated 3D Printed Sample

Apart from calculating the amount of electrodeposited copper and zinc through current measurements, the approach with weighting the 3D printed sample was also used. The data can be seen in Table 6.1.

Table 6.1: Table with the weight measurements of the 3D printed sample at different stages during the electrodeposition process; the initial weight is displayed at the far left followed by the difference in the weight at each stage

Process	After Printing	After Ethanol Bath	After Silver Paste	After Immersion in Copper Solution	After Copper Electrodeposition	After Zinc Electrodeposition
Weight	5.34g	+0.02g	+0.20g	+0.24g	+0.05g	-0.13g

However, as can be seen in Table 6.1, the weighting of the 3D printed sample was futile as the weight of the 3D printed sample decreased significantly after the zinc electrodeposition; a difference of 0.13 g was observed. Thus, the only explanation for such a difference in the weight can obtained from observing the physical condition of the 3D printed sample. A picture after the zinc electrodeposition can be seen in Figure 6.8.

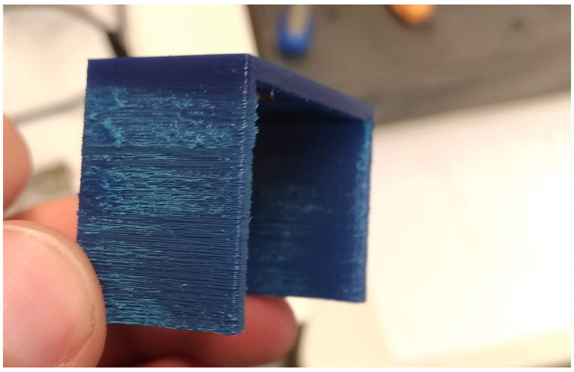

Figure 6.8: A sideways picture of the 3D printed sample after zinc electrodeposition; notice the discoloration of the layers towards the top of the print

As can be seen in Figure 6.8, there is a visible discoloration in the structure of the 3D printed sample, particularly noticeable along the top portion. Such discoloration can be attributed to the known corrosive properties of the sulfuric acid and sulfate ions that are present in both baths. For future reference, there is a research paper on the chemical compatibility of 3D printer filament with solutions commonly used in chemical laboratory experiments [Heikkinen et al., 2018]. The research paper ultimately drew the conclusion that PLA is poorly compatible with sulfuric acid as it dissolves completely over time.

6.2 Electrochemical Impedance Analysis

During the electrochemical impedance analysis measurements, the LCR meter stated in Chapter 5 was used to acquire the measurements in Figure 6.9. As mentioned in Chapter 4, an equivalent circuit of the battery based on the Randles Model can be made from the impedance data.

Unfortunately, due to the issue of time, only one LCR measurement run was conducted. In Figure 6.9, the magnitude and phase of the impedance of the 3D printed battery was plotted against frequency. In Figure 6.10, a Cole-Cole plot of the data measured by the LCR meter can be seen. In Figure 6.11, the Nyquist plot of the data captured by the LCR meter can be seen.

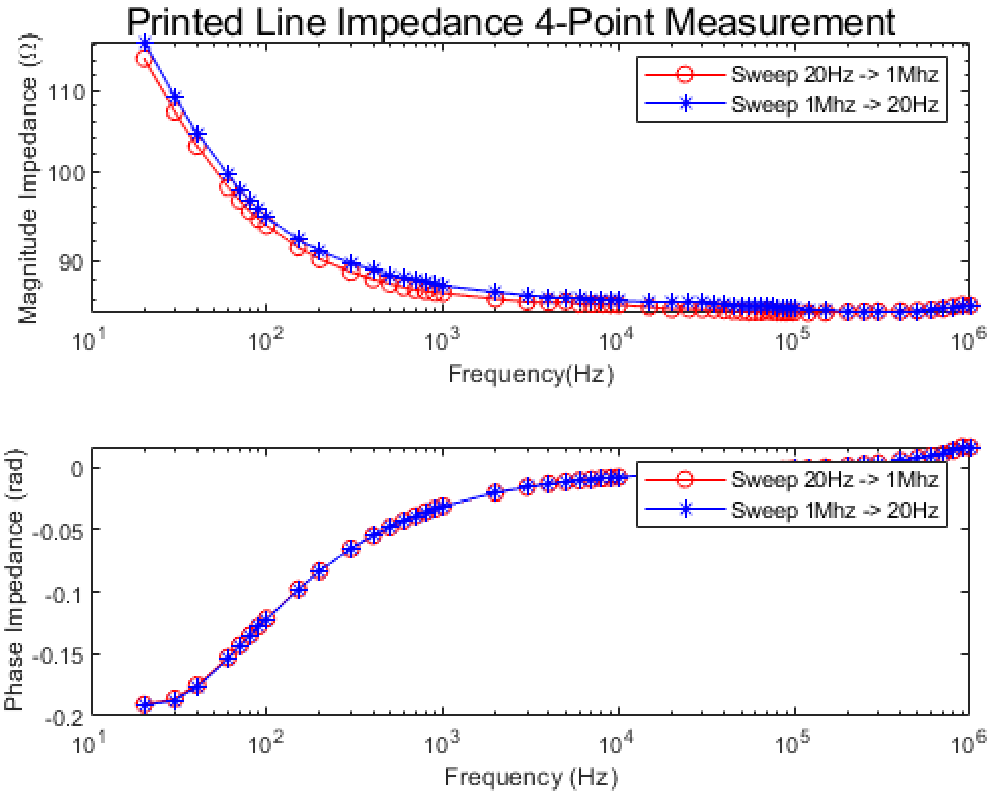

Figure 6.9: A graph with the magnitude and phase of the impedance of the 3D printed battery plotted against frequency from 20 Hz to 1 MHz

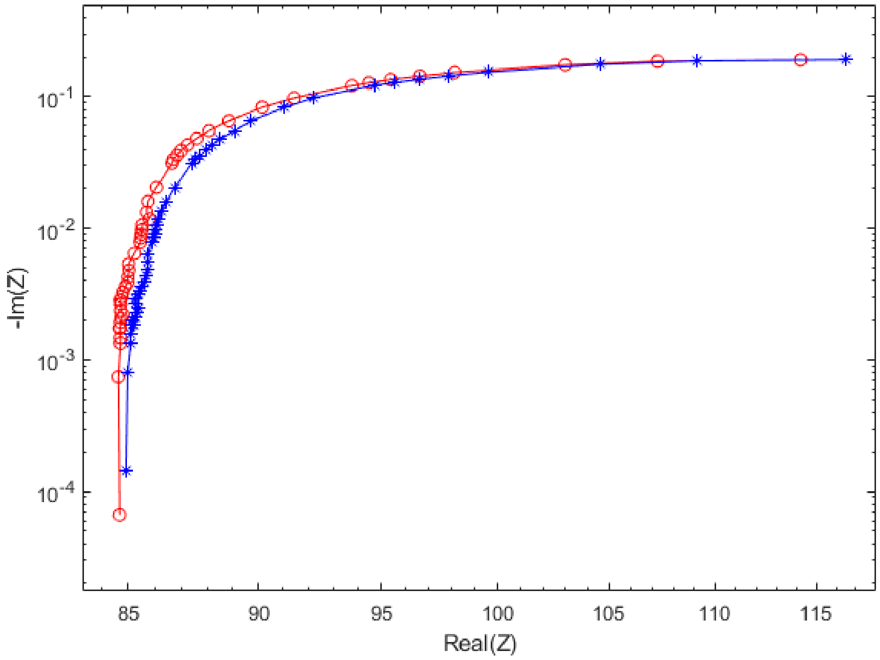

Figure 6.10: A Cole-Cole plot with the real impedance plotted against the logarithmic of the imaginary impedance

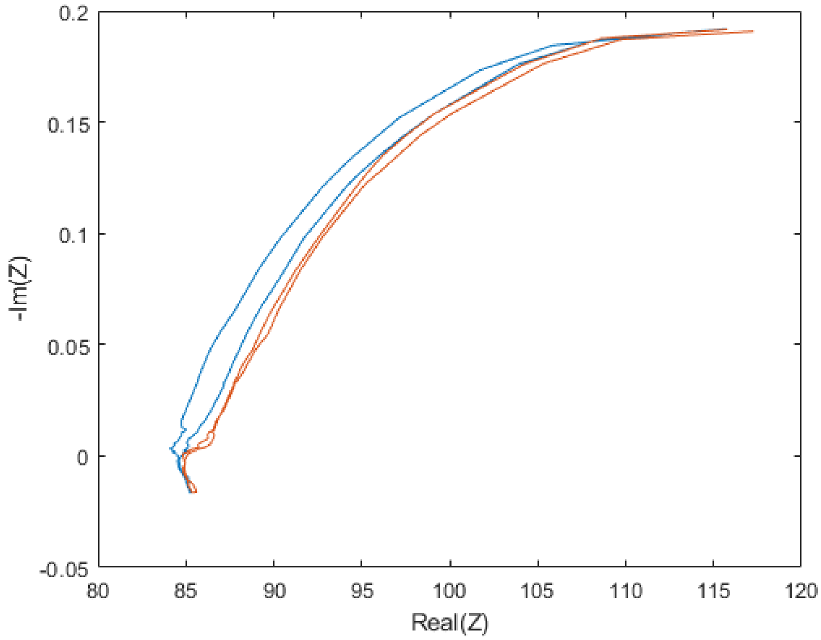

Figure 6.11: A Nyguist plot of the 3D printed battery

From a glance at all three plots, the results are not what was expected as the graphs do not match or resemble anything from the research papers on electrochemical impedance spectroscopy of batteries [Shih and Lo, 1996, ele, 2019, Ramasamy, 2013].

Unfortunately, with the available dataset and knowledge, it was not possible to make any conclusions.

6.3 Battery Discharge Test

Once it had been measured with the LCR meter, the 3D printed battery was attached to a load of 1 Ω and left to discharge. As mentioned in Chapter 5, a multimeter was used as an ammeter and was connected in series with the load and the battery.

As reference for comparison later, the voltage potential of the 3D printed battery was measured without the load attached. The voltage potential can be seen in Figure 6.12.

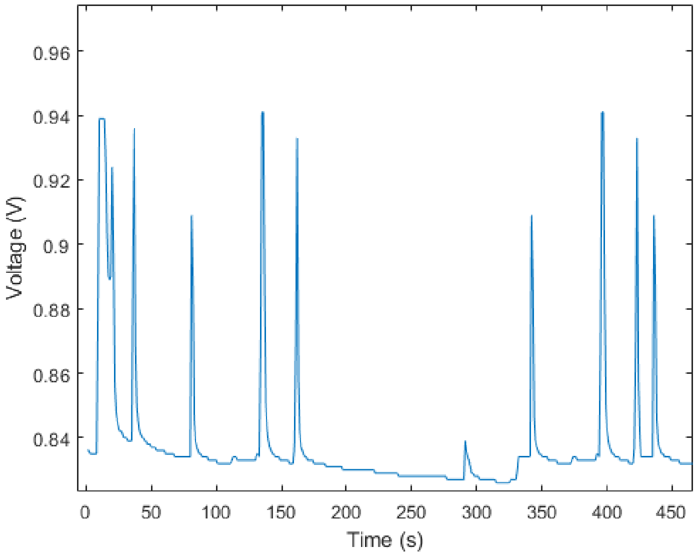

Figure 6.12: A graph of the voltage potential of the 3D printed battery without a load attached

As can be seen in Figure 6.12, the voltage potential is approximately 0.835 V, or 0.065 V under the expectation of 0.9 V as stated in Chapter 3. Regarding the sharp spikes in Figure 6.12, an interesting observation was be made. The spikes in the voltage values are directly related to the application of force to the electrical tape holding the wires in place on the 3D printed battery. Therefore, the voltage potential of the 3D printed battery reacted positively to external stimulus.

In Figure 6.13, the current measurement of the 3D printed battery over the course of its discharge cycle can be seen. Additionally, with regards to Ohm's Law, the current measurement graph in Figure 6.13 is also the voltage measurement graph since the resistor has a value of 1 Ω.

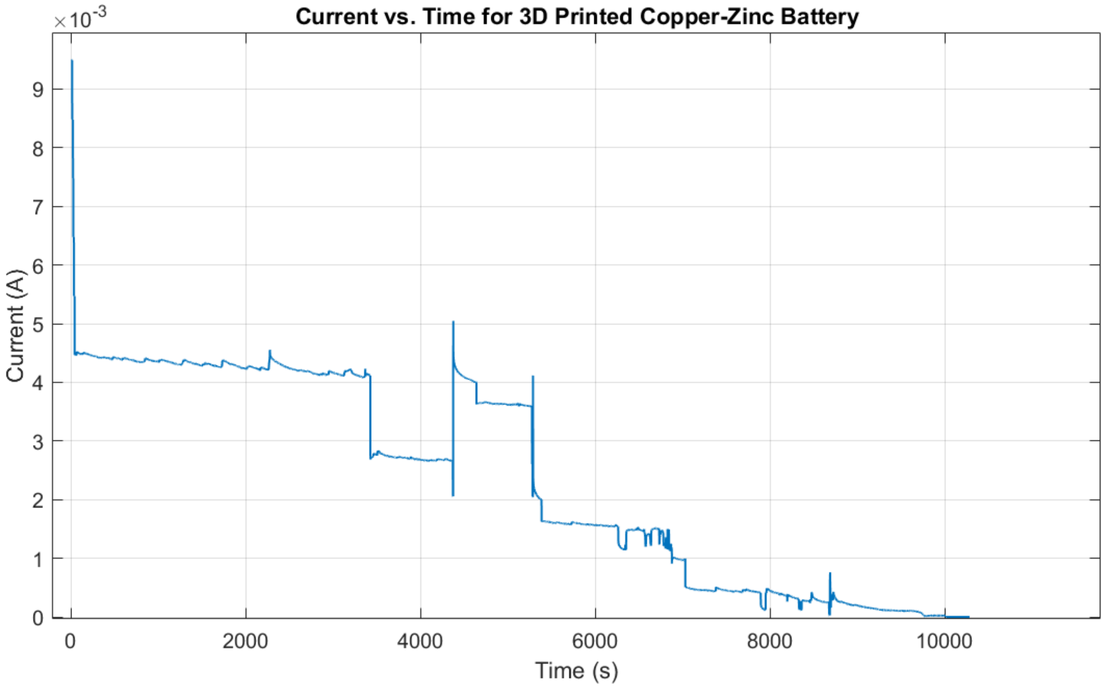

Figure 6.13: A graph of the current measurements of the 3D printed battery attached to load of 1 Ω

As once can see from the horizontal axis in Figure 6.13, the entire measurement took approximately 171 min and 20 s, or a total of 2 h, 51 min, and 20 s. The initial discharge measurement run has to be discarded as it was not known that the multimeter has a maximum save data interval of 1028 s, or 17.133 min.

It is not known what effect the repeated electrodeposition of zinc has on the capacity of the 3D printed battery. Due to the constraint of time, no more current and voltage measurements of the battery discharge cycle were conducted.

Then, by taking the integral of the current over time, the capacity of the 3D printed battery can be calculated as follows:

$$\text{Capacity} = \int_0^T I\,dt = \int_0^{10280} I\,dt = 24\,\text{mA}\cdot\text{s}\cdot\frac{1\,\text{min}}{60\,\text{s}}\cdot\frac{1\,\text{h}}{60\,\text{min}} = 6.6\,\text{mA}\cdot\text{h} \tag{6.9}$$

Thus, the capacity of the battery is rated at 6.6 mA·h. To increase the capacity of the battery, the amount of zinc electrodeposited should be increased as the redox reactions cease once the zinc metal on the electrode has completely oxidized.

Due to the constraint of time, further battery discharge tests with increased capacity could not be conducted.

On a side note, the small variations in the current, particularly after the 6000 s mark, are indentations in time when the tapes holding the wires connected to the topside of the electrodes became undone and had to be reapplied through the application of force.

Moreover, in Figure 6.13, one can see sharp drops in the current at around the 3400 s and the 5200 s mark as well as a sharp peak at around the 4300 s mark. These significant swings in the current can be attributed to the accumulation of hydrogen bubbles along the underside of the electrodes as can be seen in Figure 6.14.

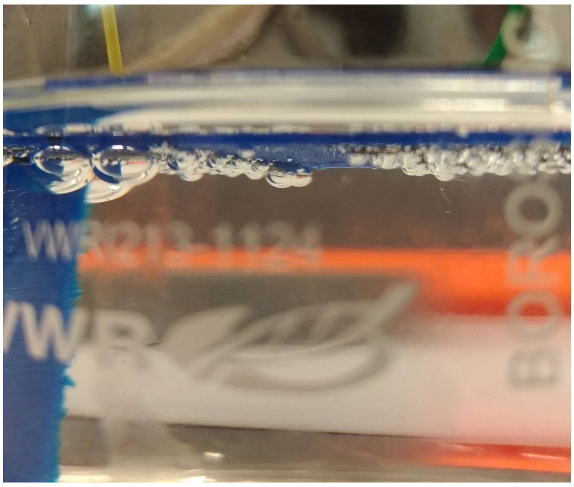

Figure 6.14: A picture of the underside of the 3D printed battery immersed in the citric acid electrolyte; the left side is the zinc electrode and the right side is the copper electrode

The formation of the hydrogen bubbles are an indication that the hydrogen ions from the electrolyte are being reduced. However, the accumulation of hydrogen bubbles should only occur at the copper cathode, where the electrons from the oxidation of the zinc electrode gather. The only sound explanation is that the zinc electrode is acting as a multi-electrode due to the fact that both oxidation and reduction occur on its surface simultaneously [Ahmad, 2006]. Normally, the external part of the circuit, the wire in this case, allows the passage of electrons from the zinc anode to the copper cathode. **Thus, it can be inferred that the electrons released from the oxidation of the zinc metal have a stronger tendency to bond with the hydrogen ions than to pass through the more resistive 3D printed electrode.**

However, the overall lower than expected voltage measurement is not entirely explained by the presence of the hydrogen bubbles. Since a 1 Ω resistor was used as the load, the expected value for the current flowing through the measurement setup should have initially been in the same range as the value of the voltage potential measured in Figure 6.12. As can be observed from Figure 6.13, there is a discrepancy in the units of the current by a factor of 100.

Therefore, the current measured by the measurement setup can only be explained by the presence of additional resistance somewhere in the circuit. Thus, the only conclusion that can be drawn is the additional resistance is coming from the internal resistance of the battery. However, without proper data from the LCR meter, it cannot verified and supported by measurements.

6.3.1 Other Observations

As the 3D printed battery was a primary cell, the 3D printed sample had to undergo electrodeposition once discharged. Fortunately, since the copper is not used up in the redox reactions, it is only necessary to electrodeposit the zinc again and replace the electrolyte. In Figure 6.15, a picture of the underside of the 3D printed sample can be seen after the 3D printed battery has been fully discharged; the copper remains while all the electrodeposited zinc has undergone oxidation and only the electrically conductive 3D printed electrode remains.

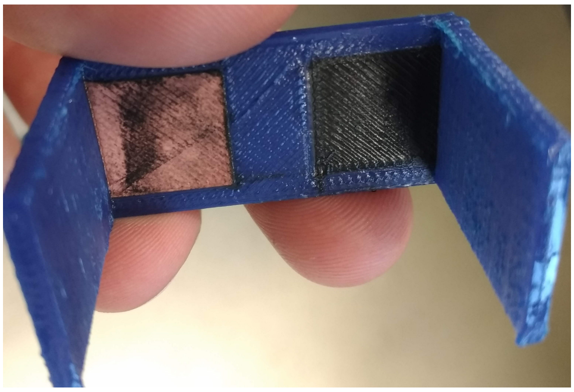

Figure 6.15: A picture of the 3D printed sample after the zinc metal has been entirely depleted

Furthermore, an important observation is that the copper begins to oxidize after a few days in an open-air environment. Additionally, the citric acid electrolyte evaporates over time and is prone to mold growth, if left unattended for long periods of time.

In the following chapter, the conclusion will be provided where the research questions stated in the introduction will be answered. In addition, future areas for improvement will be presented.

7 Conclusion

In the end, the 3D printed battery was successfully fabricated through the use of electrodeposition. However, the measured performance was far from expectation in comparison with calculated predictions and other currently researched batteries.

3D printing of batteries is a rapidly growing scientific field that has shown potential to showcase exciting new results. To fully understand the electrical and chemical properties that happen within 3D printed batteries, better measurement methods and equipment setups have to researched and implemented.

The main research question that were stated in Chapter 1 can be answered, along with the subquestions:

- **How does the performance of a 3D printed battery fabricated with the use of electrodeposition compare with currently researched batteries?**

Overall, the performance of the 3D printed battery was very poor. First of all, the average voltage during the entire discharge cycle of the 3D printed battery was 2.36 mV. During the first 4000 s, the nominal voltage was 4.4 mV at its best. On the other hand, the carbon-zinc battery achieved a nominal voltage of approximately 1.6 V [Alias and Mohamad, 2015]. The lithium titanium oxide and lithium manganese oxide batteries achieved a nominal voltage of roughly 1.5 V and 3.2 V, respectively [Reyes et al., 2018]. Secondly, the specific capacity was calculated to be 1.109 $\mathrm{mA\,h\,g^{-1}}$ with only the mass of the 3D printed sample considered. The specific capacity shrunk to 0.022 $\mathrm{mA\,h\,g^{-1}}$ when the 3D printed sample and citric acid electrolyte were considered. Both values pale in comparison to the specific capacity of the zinc-carbon battery with the value of 300 $\mathrm{mA\,h\,g^{-1}}$ [Alias and Mohamad, 2015]. Likewise, considering only the surface of the zinc electrode, the specific capacity of the 3D printed battery was calculated to be 2.93 $\mathrm{mAh/cm^2}$. Moreover, the two 3D printed lithium batteries are more energy dense, are rechargeable, and can deliver almost seven times the current compared to the 3D printed battery of this thesis in some cases. Thus, there is room for a lot of improvement.

- **What is the optimal configuration of the 3D printed electrodes that will permit the best coverage of metal ions during the electrodeposition process?**

The optimal configuration for the 3D printed electrodes is the path of least resistance. Ideally, the electrodes would be infinitesimally thin and infinitely long and wide. Furthermore, it is important that the electrodes have an unobstructed access to the electroplating solution. Thanks to the advantage of having a magnetic stirrer, the effects of the stagnation of the metal ions in the electroplating solution is not an issue. Additionally, the area of the electrodes that is to be electroplated should ideally be facing the counter electrode so that the surface is in the path of the electric field lines and captures a greater surface area of the electric flux.

- **What is the ideal electrolyte that will allow for the largest battery capacity?**

As seen in Chapter 6, the capacity of the 3D printed battery relies on the combination of the amount of zinc electrodeposition and the size of the electrolyte. In the case of the 3D printed battery fabricated in this thesis, the supply of zinc depletes before the supply of citric acid electrolyte. Thus, in this case, an increase in the amount of electrodeposited zinc metal would increase the capacity of the 3D printed battery.

In the case that the supply of zinc metal was not the issue, the ideal electrolyte would be sulfuric acid as mentioned in Chapter 3. However, sulfuric acid would have the highest cell voltage, but it would be the measure of the concentration of the acid that would determine which acid has the largest capacity [Wikipedia contributors, 2019h].

- **How can the electrical characteristics of the 3D printed battery be modelled?**

Unfortunately, the data measurements from the LCR meter were inconclusive. The curves on the Cole-Cole plot, the Nyquist plot, and the impedance magnitude and phase plot did not closely resemble anything presented by other research papaers [Shih and Lo, 1996, Ramasamy, 2013, ele, 2019].

7.1 Future Research

In terms of future improvements and research questions, there are quite a few.

For one, further research could be devoted to implementing a porous membrane through 3D printing into a double cell battery. Layfomm is a potential candidate for the porous membrane due to its unique composition of part rubber-elastomeric polymer and part PVA. Then, using the Diabase 3D printer, which the capability of printing six different materials at once, the Proto-Pasta, PLA, and Layfomm can be printed at the same time.

Furthermore, research could be directed towards the fabrication of a secondary battery in the form of a nickel-zinc metal pair. There are numerous research papers that have already proven the lithium can be electroplated.

Future improvements in regards to the research in this thesis can be made in selecting more corrosive resistant materials. However, from the table of materials in Chapter 3, the only other option for the type of electrically conductive material is ETPU. Further research could be done to explore the chemical compatibility of materials such as carbon fiber and graphene.

Moreover, the design of the 3D printed battery could be modified such that the electrolyte is contained within the 3D printed battery rather than an external container like a glass beaker.

For the measurement of the battery discharge cycle, other measurement devices such as electronic load devices and power supplies could also be considered.

A Matlab Code

A.1 Electrodeposition

```
clear all
close all

sourcemeter = keithley_2410_serial_init(3);

fs = 2; %Hz
secPerA = 10e6;%s/A
slope = 1/secPerA;%A/s
Imax = 10e-6;
Imin = -10e-6;
compliance = 12;
n = 5;

tend = (Imax-Imin)*2*n*secPerA/60

dI = slope/fs;
I = [0:dI:Imax,Imax:-dI:Imin,Imin:dI:0];
n2 = length(I);
I(1:803) = 45e-3;


tic
i1 = 1;
figure
h1 = animatedline;
ylabel('voltage(V)')
xlabel('time(sec))')

for i1 = 1:n
    for i2 = 1:n2
        i3 = (i1-1)*n2+i2;
        keithley_2410_serial_source_current_4wire(
           sourcemeter,I(i2),compliance)
        [voltage(i3),current(i3)] =
           keithley_2410_serial_read(sourcemeter);
        time(i3) = toc;

        addpoints(h1,time(i3),current(i3));
        drawnow
        if i3 > 2
            axis([min(time),max(time), min(current),max(
               current)]);
        end
    end
    i1
end
```

```
load counter
save(['data',mat2str(counter),'.mat'],'voltage', 'current'
   ,'time')
counter = counter + 1;
save('counter.mat','counter');

fclose(sourcemeter)
```

A.2 LCR Meter

```
clear all
close all

Range = {''}
sweeps = 2;%number of frequency sweeps
 frequencies = [20 30 40 60 70 80 90 100 150 200 300 400
    500 600 700 800 900 1000 2000 3000 4000 5000 6000 7000
     8000 9000 10000 15000 20000 25000 30000 35000 40000
    45000 50000 55000 60000 65000 70000 75000 8e4 8.5e4 9
    e4 9.5e4 1e5 1.2e5 1.5e5 2e5 2.5e5 3e5 4e5 5e5 6e5 7e5
     8e5 9e5 1e6];
% frequencies = fliplr(frequencies);
frequencies = [frequencies fliplr(frequencies)];
bias = 0;
frequs = length(frequencies);%number of frequencies

GPIB_adress = 17;
RLCmeter = HP4284A_init(GPIB_adress);

tic
for i2 = 1:sweeps
    for i1 = 1:frequs
        tempdata = HP4284A_single(RLCmeter,frequencies(i1)
           ,10e-3,bias,'ZTR','LONG',1);
        if ~isempty(tempdata)
            Rp(i1,i2) = tempdata(2);
            Cp(i1,i2) = tempdata(1);
        else
            Rp(i1,i2) = 0;
            Cp(i1,i2) = 0;
            disp('error')
        end
        time(i1,i2) = toc;
        i2
        i1
    end
end


load counter
```

```
save(['CPRPdata',mat2str(counter),'.mat'],'Rp', '
   frequencies','Cp','bias','time')
counter = counter + 1;
save('counter.mat','counter');

fclose(RLCmeter)
%%
for i1 = 1:size(Cp,1);
    for i2 = 1:size(Cp,2);
        if Cp(i1, i2) >1e10
            Cp(i1, i2) = nan;
        end

        if abs(Rp(i1, i2))>2*pi
            Rp(i1, i2) = nan;
        end
    end
end

dim = 2;
avgRp = mean(Rp,dim);
stdRp = std(Rp,0,dim);
avgCp = mean(Cp,dim);
stdCp = std(Cp,0,dim);

figure
subplot(2,1,1)
errorbar(log10(frequencies),avgCp,stdCp)
xlabel('log(Frequency) (Hz)')
ylabel('Magnitude Impedance (\Omega)')

subplot(2,1,2)
errorbar(log10(frequencies),avgRp,stdRp)
xlabel('log(Frequency) (Hz)')
ylabel('Phase Impedance (rad)')

figure
col = parula(sweeps);
% col = jet(sweeps);

for i1 = 1:sweeps
    subplot(2,1,1);
    loglog(frequencies,Cp(:,i1), 'o-', 'Color', col(i1,:))
       ;
    xlabel('Frequency(Hz)')
    ylabel('Magnitude Impedance (\Omega)')
    hold on
    subplot(2,1,2)
    semilogx(frequencies,Rp(:,i1), 'o-', 'Color', col(i1
       ,:))
    xlabel('Frequency (Hz)')
```

```
    ylabel('Phase Impedance (rad)')
    hold on
end

% colormap jet
subplot(2,1,1);
caxis([1 sweeps]);
h1= colorbar;
subplot(2,1,2)
caxis([1 sweeps]);
h2= colorbar;

%% Back-and-forth sweep
% figure
% for i1 = 1:sweeps
%     subplot(2,1,1);
%     loglog(frequencies(1:length(frequencies)/2),Cp(1:
   length(frequencies)/2,i1), 'ro-');
%     xlabel('Frequency(Hz)')
%     ylabel('Magnitude Impedance (\Omega)')
%     hold on
%     loglog(frequencies(length(frequencies)/2+1:end),Cp(
   length(frequencies)/2+1:end,i1), 'b*-')
%     subplot(2,1,2)
%     semilogx(frequencies(1:length(frequencies)/2),Rp(1:
   length(frequencies)/2,i1), 'ro-')
%     xlabel('Frequency (Hz)')
%     ylabel('Phase Impedance (rad)')
%     hold on
%     semilogx(frequencies(length(frequencies)/2+1:end),Rp
   (length(frequencies)/2+1:end,i1), 'b*-')
% end

meanCplr = nanmean(Cp(1:length(frequencies)/2,:)');
meanCprl = nanmean(Cp(length(frequencies)/2+1:end,:)');
meanRplr = nanmean(Rp(1:length(frequencies)/2,:)');
meanRprl = nanmean(Rp(length(frequencies)/2+1:end,:)');

figure
suptitle('Printed Line Impedance 4-Point Measurement')
subplot(2,1,1);
    loglog(frequencies(1:length(frequencies)/2),meanCplr,
       'ro-');
    xlabel('Frequency(Hz)')
    ylabel('Magnitude Impedance (\Omega)')
    hold on
    loglog(frequencies(length(frequencies)/2+1:end),
       meanCprl, 'b*-')
    legend('Sweep 20Hz -> 1Mhz', 'Sweep 1Mhz -> 20Hz')
    subplot(2,1,2)
```

```
    semilogx(frequencies(1:length(frequencies)/2),meanRplr
       , 'ro-')
    xlabel('Frequency (Hz)')
    ylabel('Phase Impedance (rad)')
    hold on
    semilogx(frequencies(length(frequencies)/2+1:end),
       meanRprl, 'b*-')
    legend('Sweep 20Hz -> 1Mhz', 'Sweep 1Mhz -> 20Hz')

% %% Plot colour gradient
% N = length(frequencies);
% col = parula(N);
%
% figure
% for i = 1:N
%     subplot(2,1,1)
%     loglog(frequencies([i i+1]), Cp([i i+1]), 'o-', '
   color', col(i,:))
%     hold on
%     colorbar
%     subplot(2,1,2)
%     semilogx(frequencies([i i+1]), Rp([i i+1]), 'o-', '
   color', col(i,:))
%     hold on
% end
```

B Dimensions of 3D Printed Sample

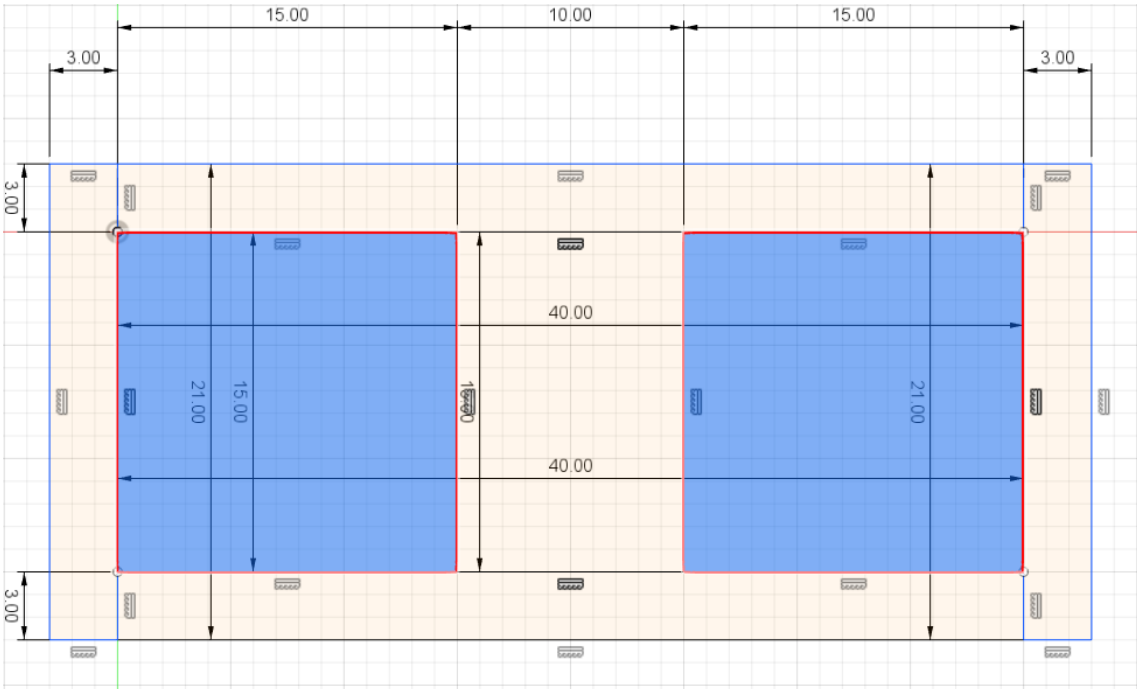

Figure B.1: A picture of the Autodesk Fusion 360 sketch of the 3D printed battery

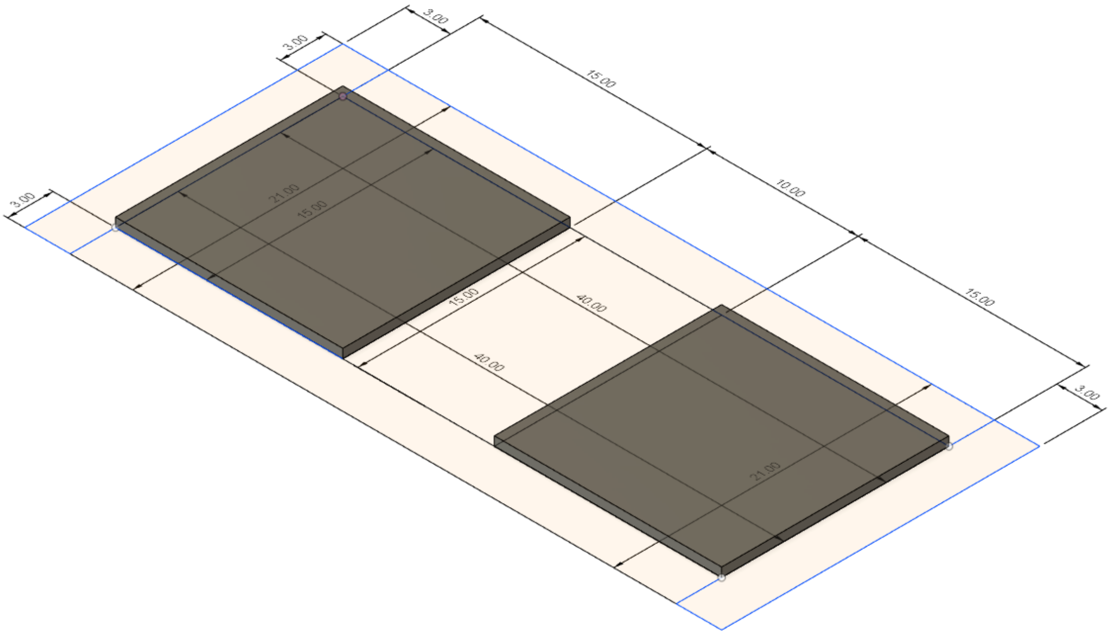

Figure B.2: A picture of the AutoDesk Fusion 360 models of the two electrodes with a thickness of 6mm

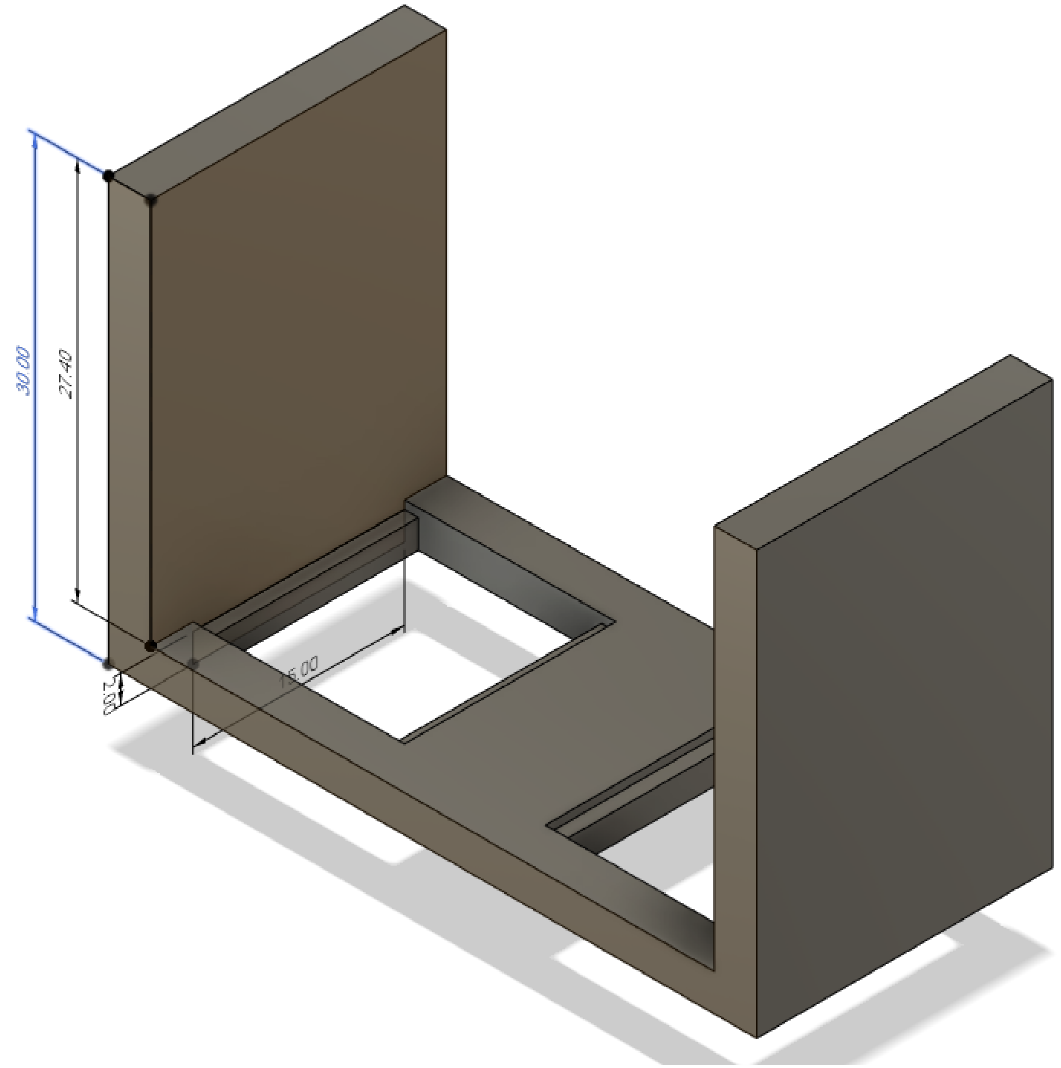

Figure B.3: A picture of the AutoDesk Fusion 360 model of the housing of the electrodes

Bibliography

[pro, 2017] (2017), Electrically Conductive Composite PLA. https://www.proto-pasta.com/collections/exotic-composite-pla/products/conductive-pla?variant=1265211476

[ele, 2019] (2019), Basics of Electrochemical Impedance Spectroscopy. https://www.gamry.com/application-notes/EIS/basics-of-electrochemical-impedance-spectroscopy/

[cit, 2019] (2019), Citric acid 251275. https://www.sigmaaldrich.com/catalog/product/sial/251275?lang=en&region=NL

[1bu, 2019] (2019), Renewable energy is costing less than fossil fuels, says Michael Milken. https://1businessworld.com/2019/09/business/renewable-energy-is-cost-effective-says-michael-milken-html/

[Ahmad, 2006] Ahmad, Z. (2006), CHAPTER 3 - CORROSION KINETICS, in *Principles of Corrosion Engineering and Corrosion Control*, Ed. Z. Ahmad, Butterworth-Heinemann, Oxford, pp. 57 – 119, ISBN 978-0-7506-5924-6, doi:https://doi.org/10.1016/B978-075065924-6/50004-0. http://www.sciencedirect.com/science/article/pii/B9780750659246500040

[Alias and Mohamad, 2015] Alias, N. and A. A. Mohamad (2015), Morphology study of electrodeposited zinc from zinc sulfate solutions as anode for zinc-air and zinc-carbon batteries, **vol. 27**, no.1, p. 43–48, doi:10.1016/j.jksues.2013.03.003.

[Angel et al., 2018] Angel, K., H. H. Tsang, S. S. Bedair, G. L. Smith and N. Lazarus (2018), Selective electroplating of 3D printed parts. https://www.sciencedirect.com/science/article/pii/S2214860417305353

[Bart, 2009] Bart, J. (2009), PhD Report: Stripline-based microfluidic devices for high-resolution NMR spectroscopy, doi:10.3990/1.9789036528986.

[Beidaghi and Gogotsi, 2014] Beidaghi, M. and Y. Gogotsi (2014), Capacitive energy storage in micro-scale devices: recent advances in design and fabrication of micro-supercapacitors, **vol. 7**, no.3, p. 867, doi:10.1039/c3ee43526a.

[Blake et al., 2017] Blake, A. J., R. R. Kohlmeyer, J. O. Hardin, E. A. Carmona, B. Maruyama, J. D. Berrigan, H. Huang and M. F. Durstock (2017), 3D Printable Ceramic-Polymer Electrolytes for Flexible High-Performance Li-Ion Batteries with Enhanced Thermal Stability, **vol. 7**, no.14, p. 1602920, doi:10.1002/aenm.201602920.

[Dhole et al., 2018] Dhole, I. A., Y. H. Navale, C. S. Pawar, S. T. Navale and V. B. Patil (2018), Physicochemical and supercapacitive properties of electroplated nickel oxide electrode: effect of solution molarity, **vol. 29**, no.7, p. 5675–5687, doi:10.1007/s10854-018-8537-y.

[Dijkshoorn et al., 2019] Dijkshoorn, A., M. Schouten, G. Wolterink, R. Sanders and G. Krijnen (2019), Characterizing the Electrical Properties of Anisotropic, 3D-Printed Conductive Sheets, *2019 IEEE International Conference on Flexible and Printable Sensors and Systems (FLEPS)*, doi:10.1109/fleps.2019.8792279.

[Down et al., 2019] Down, M. P., E. Martínez-Periñán, C. W. Foster, E. Lorenzo, G. C. Smith and C. E. Banks (2019), Next-Generation Additive Manufacturing of Complete Standalone Sodium-Ion Energy Storage Architectures, **vol. 9**, no.11, p. 1803019, doi:10.1002/aenm.201803019.

[Dudley, 2018] Dudley, D. (2018), Renewable Energy Will Be Consistently Cheaper Than Fossil Fuels By 2020, Report Claims.
`https://www.forbes.com/sites/dominicdudley/2018/01/13/renewable-energy-cost-effective-fossil-fuels-2020/`

[Editors, 2019] Editors, R. E. W. (2019), BNEF: Energy to storage increase 122X by 2040.
`https://www.renewableenergyworld.com/2019/07/31/bnef-energy-storage-increase-122x-by-2040/`

[Esfandiari et al., 1983] Esfandiari, R., D. Maki and M. Siracusa (1983), Design of Interdigitated Capacitors and Their Application to Gallium Arsenide Monolithic Filters, **vol. 31**, no.1, p. 57–64, doi:10.1109/tmtt.1983.1131429.

[Felloni et al., 1987] Felloni, L., R. Fratesi, E. Quadrini and G. Roventi (1987), Electrodeposition of zinc-nickel alloys from chloride solution, **vol. 17**, no.3, p. 574–582, doi:10.1007/bf01084132.

[FlashForge, 2017] FlashForge (2017), Flashforge Creator Pro User Manual.
`https://www.manualslib.com/manual/1205097/Flashforge-Creator-Pro.html`

[Garay and Bashirullah, 2015] Garay, E. F. and R. Bashirullah (2015), Biofluid Activated Microbattery for Disposable Microsystems, **vol. 24**, no.1, p. 70–79, doi:10.1109/jmems.2014.2317177.

[Guy, 2004] Guy (2004), sciphile.org.
`http://sciphile.org/lessons/survey-homemade-batteries`

[Heikkinen et al., 2018] Heikkinen, I. T., C. Kauppinen, Z. Liu, S. M. Asikainen, S. Spoljaric, J. V. Seppälä, H. Savin and J. M. Pearce (2018), Chemical compatibility of fused filament fabrication-based 3-D printed components with solutions commonly used in semiconductor wet processing, *Additive Manufacturing*, **vol. 23**, p. 99–107, doi:10.1016/j.addma.2018.07.015.

[Ho et al., 2009] Ho, C. C., K. Murata, D. A. Steingart, J. W. Evans and P. K. Wright (2009), A super ink jet printed zinc–silver 3D microbattery, **vol. 19**, no.9, p. 094013, doi:10.1088/0960-1317/19/9/094013.

[Kadari, 2017] Kadari, K. K. (2017), MSc Report: Electroplating on 3D Printed Conductive Track.

[Kanani, 2006] Kanani, N. (2006), *Electroplating: basic principles, processes and practice*, Elsevier, ISBN 9781856174510.

[Keithley, 2014] Keithley (2014), Series 2400 SourceMeter SMU Instruments.
`https://nl.farnell.com/keithley/2410/meter-sourcemeter-1100v/dp/2074738`

[Keysight, 2019] Keysight (2019), Digital Multimeters 34460A, 34461A, 34465A ($6\frac{1}{2}$ digit), 34470A ($7\frac{1}{2}$ digit).
`https://literature.cdn.keysight.com/litweb/pdf/5991-1983EN.pdf?id=2318052&cc=NL&lc=dut`

[Kim et al., 2016] Kim, J., R. Kumar, A. J. Bandodkar and J. Wang (2016), Advanced Materials for Printed Wearable Electrochemical Devices: A Review, **vol. 3**, no.1, p. 1600260, doi:10.1002/aelm.201600260.

[Kim et al., 2019] Kim, M. J., M. A. Cruz, S. Ye, A. L. Gray, G. L. Smith, N. Lazarus, C. J. Walker, H. H. Sigmarsson and B. J. Wiley (2019), One-step electrodeposition of copper on conductive 3D printed objects, *Additive Manufacturing*, **vol. 27**, p. 318–326, doi:10.1016/j.addma.2019.03.016.

[Lawes et al., 2015] Lawes, S., A. Riese, Q. Sun, N. Cheng and X. Sun (2015), Printing nanostructured carbon for energy storage and conversion applications, *Carbon*, **vol. 92**, p. 150–176, doi:10.1016/j.carbon.2015.04.008.

[Liu et al., 2017] Liu, C., X. Cheng, B. Li, Z. Chen, S. Mi and C. Lao (2017), Fabrication and Characterization of 3D-Printed Highly-Porous 3D LiFePO4 Electrodes by Low Temperature Direct Writing Process, **vol. 10**, no.8, p. 934, doi:10.3390/ma10080934.

[Mcowen et al., 2018] Mcowen, D. W., S. Xu, Y. Gong, Y. Wen, G. L. Godbey, J. E. Gritton, T. R. Hamann, J. Dai, G. T. Hitz, L. Hu and et al. (2018), 3D-Printing Electrolytes for Solid-State Batteries, **vol. 30**, no.18, p. 1707132, doi:10.1002/adma.201707132.

[Pickerel et al., 2019] Pickerel, K., K. Pickerel, Solarman and Solarman (2019), U.S. Congress introduces "Better Energy Storage Technology" Act to increase battery RD.
`https://www.solarpowerworldonline.com/2019/05/`
`u-s-congress-introduces-better-energy-storage-technology-act-to-increase-`

[Pocket-lint, 2019] Pocket-lint (2019), Future batteries, coming soon: Charge in seconds, last months and power over the air.
`https://www.pocket-lint.com/gadgets/news/`
`130380-future-batteries-coming-soon-charge-in-seconds-last-months-and-pow`

[Ramasamy, 2013] Ramasamy, N. S. R. P. (2013), Electrochemical Impedance Spectroscopy for Microbial Fuel Cell Characterization, *Journal of Microbial Biochemical Technology*, doi:10.4172/1948-5948.s6-004.

[Reyes et al., 2018] Reyes, C., R. Somogyi, S. Niu, M. A. Cruz, F. Yang, M. J. Catenacci, C. P. Rhodes and B. J. Wiley (2018), Three-Dimensional Printing of a Complete Lithium Ion Battery with Fused Filament Fabrication, *ACS Applied Energy Materials*, doi:10.1021/acsaem.8b00885.

[Rocha et al., 2017] Rocha, V. G., E. García-Tuñón, C. Botas, F. Markoulidis, E. Feilden, E. D'Elia, N. Ni, M. Shaffer and E. Saiz (2017), Multimaterial 3D Printing of Graphene-Based Electrodes for Electrochemical Energy Storage Using Thermoresponsive Inks, **vol. 9**, no.42, p. 37136–37145, doi:10.1021/acsami.7b10285.

[Schouten, 2017] Schouten, M. (2017), MSc Report: Towards Additively Manufactured Complex Robotic Systems, *Robotics and Mechatronics*.

[Shen et al., 2017] Shen, K., H. Mei, B. Li, J. Ding and S. Yang (2017), 3D Printing Sulfur Copolymer-Graphene Architectures for Li-S Batteries, **vol. 8**, no.4, p. 1701527, doi:10.1002/aenm.201701527.

[Shih and Lo, 1996] Shih, H. and T.-C. Lo (1996), Electrochemical Impedance Spectroscopy for Battery Research and Development.
`https://www.ameteksi.com/-/media/ameteksi/download_links/`
`documentations/library/solartonanalytical/electrochemistry/`
`technicalreport31hongshiheisforbatteryresearch.pdf?la=en`

[Sonavane et al., 2010] Sonavane, A., A. Inamdar, P. Shinde, H. Deshmukh, R. Patil and P. Patil (2010), Efficient electrochromic nickel oxide thin films by electrodeposition, **vol. 489**, no.2, p. 667–673, doi:10.1016/j.jallcom.2009.09.146.

[Sun et al., 2015] Sun, G., J. An, C. K. Chua, H. Pang, J. Zhang and P. Chen (2015), Layer-by-layer printing of laminated graphene-based interdigitated microelectrodes for flexible planar micro-supercapacitors, *Electrochemistry Communications*, **vol. 51**, p. 33–36, doi:10.1016/j.elecom.2014.11.023.

[Tian et al., 2017] Tian, X., J. Jin, S. Yuan, C. K. Chua, S. B. Tor and K. Zhou (2017), Emerging 3D-Printed Electrochemical Energy Storage Devices: A Critical Review, **vol. 7**, no.17, p. 1700127, doi:10.1002/aenm.201700127.

[Tiliakos et al., 2018] Tiliakos, A., A. M. Trefilov, E. Tanas, A. Balan and I. Stamatin (2018), Space-Filling Supercapacitor Carpets: Highly scalable fractal architecture for energy storage, *Journal of Power Sources*, **vol. 384**, p. 145–155, doi:10.1016/j.jpowsour.2018.02.061.

[Vangari et al., 2013] Vangari, M., T. Pryor and L. Jiang (2013), Supercapacitors: Review of Materials and Fabrication Methods, **vol. 139**, no.2, p. 72–79, doi:10.1061/(asce)ey.1943-7897.0000102. https://ascelibrary.org/doi/abs/10.1061/(ASCE)EY.1943-7897.0000102

[Walsh et al., 2018] Walsh, F. C., L. F. Arenas and C. P. D. León (2018), Developments in electrode design: structure, decoration and applications of electrodes for electrochemical technology, **vol. 93**, no.11, p. 3073–3090, doi:10.1002/jctb.5706.

[Wang et al., 2017] Wang, Y., C. Chen, H. Xie, T. Gao, Y. Yao, G. Pastel, X. Han, Y. Li, J. Zhao, K. K. Fu and et al. (2017), 3D-Printed All-Fiber Li-Ion Battery toward Wearable Energy Storage, **vol. 27**, no.43, p. 1703140, doi:10.1002/adfm.201703140.

[Waugh, 2013] Waugh, B. (2013), Vancouver campus deploys new $5.1M 'smart grid' energy storage system. https://news.ubc.ca/2013/04/19/vancouver-campus-deploys-new-5-1m-smart-grid-energy-storage-system/

[Wikipedia contributors, 2018] Wikipedia contributors (2018), Galvanostat — Wikipedia, The Free Encyclopedia, https://en.wikipedia.org/w/index.php?title=Galvanostat&oldid=837884663, [Online; accessed 4-November-2019].

[Wikipedia contributors, 2019a] Wikipedia contributors (2019a), Beaker (glassware) — Wikipedia, The Free Encyclopedia, https://en.wikipedia.org/w/index.php?title=Beaker_(glassware)&oldid=922162603, [Online; accessed 4-November-2019].

[Wikipedia contributors, 2019b] Wikipedia contributors (2019b), Daniell cell — Wikipedia, The Free Encyclopedia, https://en.wikipedia.org/w/index.php?title=Daniell_cell&oldid=916196024, [Online; accessed 4-November-2019].

[Wikipedia contributors, 2019c] Wikipedia contributors (2019c), Electric battery — Wikipedia, The Free Encyclopedia, https://en.wikipedia.org/w/index.php?title=Electric_battery&oldid=916046536, [Online; accessed 4-November-2019].

[Wikipedia contributors, 2019d] Wikipedia contributors (2019d), Electrolysis of water — Wikipedia, The Free Encyclopedia, `https://en.wikipedia.org/w/index.php?title=Electrolysis_of_water&oldid=924446096`, [Online; accessed 4-November-2019].

[Wikipedia contributors, 2019e] Wikipedia contributors (2019e), Electroplating — Wikipedia, The Free Encyclopedia, `https://en.wikipedia.org/w/index.php?title=Electroplating&oldid=923398134`, [Online; accessed 4-November-2019].

[Wikipedia contributors, 2019f] Wikipedia contributors (2019f), Faraday's laws of electrolysis — Wikipedia, The Free Encyclopedia, `https://en.wikipedia.org/w/index.php?title=Faraday%27s_laws_of_electrolysis&oldid=924534218`, [Online; accessed 4-November-2019].

[Wikipedia contributors, 2019g] Wikipedia contributors (2019g), Gigafactory 1 — Wikipedia, The Free Encyclopedia, `https://en.wikipedia.org/w/index.php?title=Gigafactory_1&oldid=923846696`, [Online; accessed 4-November-2019].

[Wikipedia contributors, 2019h] Wikipedia contributors (2019h), Lemon battery — Wikipedia, The Free Encyclopedia, `https://en.wikipedia.org/w/index.php?title=Lemon_battery&oldid=923484288`, [Online; accessed 4-November-2019].

[Wikipedia contributors, 2019i] Wikipedia contributors (2019i), Redox — Wikipedia, The Free Encyclopedia, `https://en.wikipedia.org/w/index.php?title=Redox&oldid=924446006`, [Online; accessed 4-November-2019].

[Wikipedia contributors, 2019j] Wikipedia contributors (2019j), Supercapacitor — Wikipedia, The Free Encyclopedia, `https://en.wikipedia.org/w/index.php?title=Supercapacitor&oldid=923692549`, [Online; accessed 4-November-2019].

[Yi et al., 2018] Yi, S., B. Wang, Z. Chen, R. Wang and D. Wang (2018), A study on LiFePO4/graphite cells with built-in Li4Ti5O12 reference electrodes, **vol. 8**, no.33, p. 18597–18603, doi:10.1039/c8ra03062f.

[Yu et al., 2018] Yu, W., B. Q. Li, S. Ding and H. Liu (2018), 3D printing of interdigitated electrode for all-solid-state microsupercapacitors, **vol. 28**, no.10, p. 105014, doi:10.1088/1361-6439/aad107.

[Zekoll et al., 2018] Zekoll, S., C. Marriner-Edwards, A. K. O. Hekselman, J. Kasemchainan, C. Kuss, D. E. J. Armstrong, D. Cai, R. J. Wallace, F. H. Richter, J. H. J. Thijssen and et al. (2018), Hybrid electrolytes with 3D bicontinuous ordered ceramic and polymer microchannels for all-solid-state batteries, **vol. 11**, no.1, p. 185–201, doi:10.1039/c7ee02723k.

[Zhang et al., 2017a] Zhang, F., M. Wei, V. V. Viswanathan, B. Swart, Y. Shao, G. Wu and C. Zhou (2017a), 3D printing technologies for electrochemical energy storage, *Nano Energy*, **vol. 40**, p. 418–431, doi:10.1016/j.nanoen.2017.08.037.

[Zhang et al., 2017b] Zhang, H., H. Ning, J. Busbee, Z. Shen, C. Kiggins, Y. Hua, J. Eaves, J. Davis, T. Shi, Y.-T. Shao, J.-M. Zuo, X. Hong, Y. Chan, S. Wang, P. Wang, P. Sun, S. Xu, J. Liu and P. Braun (2017b), Electroplating lithium transition metal oxides, *Science Advances*, **vol. 3**, p. e1602427, doi:10.1126/sciadv.1602427.

[Zhang et al., 2017c] Zhang, J., B. Yang, F. Fu, F. You, X. Dong and M. Dai (2017c), Resistivity and Its Anisotropy Characterization of 3D-Printed Acrylonitrile Butadiene Styrene Copolymer (ABS)/Carbon Black (CB) Composites, **vol. 7**, no.1, p. 20, doi:10.3390/app7010020.

[Zhang et al., 2014] Zhang, X., Y. Sun, J. Song, A. Wu and X. Cui (2014), A New Model of Ultracapacitors Based on Fractal Fundamentals, *Journal of Applied Mathematics*, **vol. 2014**, p. 1–7, doi:10.1155/2014/726108.

[Zhao et al., 2014] Zhao, C., C. Wang, R. Gorkin, S. Beirne, K. Shu and G. G. Wallace (2014), Three dimensional (3D) printed electrodes for interdigitated supercapacitors, *Electrochemistry Communications*, **vol. 41**, p. 20–23, doi:10.1016/j.elecom.2014.01.013.